Title

Development and Implementation of Semiempirical Framework for Modeling Postliquefaction Shear Deformation Accumulation in Sands

Journal

Journal of Geotechnical and Geoenvironmental Engineering, 146(1)

ISSN

1090-0241

Authors

Tasiopoulou, Panagiota
Ziotopoulou, Katerina
Humire, Francisco
et al.

Publication Date

2020

DOI

10.1061/(asce)gt.1943-5606.0002179

Peer reviewed

ASCE

Development and Implementation of Semiempirical Framework for Modeling Postliquefaction Shear Deformation Accumulation in Sands

Panagiota Tasiopoulou, Ph.D.[1]; Katerina Ziotopoulou, A.M.ASCE[2]; Francisco Humire, S.M.ASCE[3]; Amalia Giannakou[4]; Jacob Chacko[5]; and Thaleia Travasarou, M.ASCE[6]

Abstract: A framework for the estimation of coseismic deformations in the postliquefaction regime is developed based on an extensive database of available cyclic undrained stress-controlled tests on clean sand samples without static shear bias, covering a wide range of relative densities. Based on fundamental experimental observations, a compliance rate is defined as the postliquefaction shear strain rate per cycle over the shear stress amplitude. Semiempirical relationships of the compliance rate as a function of relative density are developed to provide guidance for estimating postliquefaction shear strains. The proposed framework provides a basis for the calibration of advanced constitutive models capable of capturing postliquefaction strain accumulation. A calibration methodology is proposed using both existing liquefaction resistance curves and the newly developed semiempirical relationships for estimating postliquefaction shear strain accumulation. The validity of the proposed methodology is demonstrated by numerical simulations, using the PM4Sand model, of two well-documented centrifuge tests focusing on liquefaction-induced demands on engineering structures. **DOI: 10.1061/(ASCE)GT.1943-5606.0002179.**

Author keywords: Postliquefaction shear strain accumulation; Liquefaction-induced deformations; Calibration methodology.

Introduction

Liquefaction-induced ground deformation can be influenced by many factors including the properties of the liquefiable material, the imposed demand, and the boundary conditions of the system at hand. Sands undergoing cyclic loading, after liquefaction triggering, can develop limited to large levels of shear strain—herein, referred to as postliquefaction strain/deformation—depending primarily on their dilative tendency and the level of shear loading. The potential for dilatancy, which determines the level of postliquefaction strain accumulation, is commonly interpreted within the critical state concept as being a function of the relative density and the overburden stress (Casagrande 1976; Castro 1975; Bolton 1986).

Performance-based methods are increasingly being adopted for the evaluation and design of geotechnical structures affected by liquefaction (e.g., Travasarou et al. 2012) and heavily rely on reliable estimates of system displacements. Thus, the evaluation of liquefaction-induced shear deformations necessitates moving beyond the prediction of liquefaction triggering and into facilitating reliable assessments of liquefaction consequences in terms of expected deformations. Quay wall rotation, footing settlements, embankment settlements, and lateral spreading deformations are just a few examples of deformation mechanisms that are primarily shear-induced under a liquefaction regime and develop both before but also after triggering. In contrast to other liquefaction-related phenomena (triggering, effects of overburden and sloping ground conditions, and postliquefaction reconsolidation volumetric strains, etc.), a consistent framework that systematically provides guidance on coseismic postliquefaction triggering shear strain accumulation is lacking. Developing a methodology for estimating the magnitude of postliquefaction-triggering deformations—especially if liquefaction is triggered early in the earthquake—is key toward evaluating the performance and the need for mitigation strategies.

Commonly used procedures for the estimation of liquefaction-induced deformations typically rely on empirical or semiempirical relationships for the estimation of lateral spreading deformations and settlements based on case studies, large scale model tests, and field data correlations, in combination with a variety of methods to process the aforementioned data (e.g., Seed et al. 1975; Seed 1979; Hamada et al. 1987; Yasuda et al. 1992; Boulanger et al. 1995; Bartlett and Youd 1995; Shamoto et al. 1998a, b; Rauch and Martin 2000; Youd et al. 2002; Zhang et al. 2004; Yi 2010). However, most of these methods rely more on the compilation of observational and site-investigation data at the system level. While these approaches provide all encompassing solutions that incorporate various geological and boundary conditions, they do not readily allow for a separation of these effects from the fundamental constitutive response of the liquefiable materials at the element level.

Nonlinear dynamic analyses (NDAs), incorporating advanced constitutive models to capture the response of soil elements, are increasingly used in engineering practice to evaluate the seismic performance of soil and soil-structure systems affected by

[1]Geotechnical Engineer, GR8 GEO, 79 Dimitrakopoulou St., Athens 11741, Greece (corresponding author). ORCID: https://orcid.org/0000-0001-8574-5519. Email: ptasiopoulou@gr8-geo.com; ptasiopoulou@gmail.com

[2]Assistant Professor, Dept. of Civil and Environmental Engineering, Univ. of California, Davis, Davis 95616, CA.

[3]Graduate Student Researcher, Dept. of Civil and Environmental Engineering, Univ. of California, Davis, Davis 95616, CA.

[4]Principal Engineer, GR8 GEO, 79 Dimitrakopoulou St., Athens 11741, Greece. ORCID: https://orcid.org/0000-0003-0526-9925

[5]Principal Engineer, GR8 GEO, 79 Dimitrakopoulou St., Athens 11741, Greece. ORCID: https://orcid.org/0000-0003-4555-3082

[6]Principal Engineer, Fugro, 1777 Botelho Dr., Suite 262, Walnut Creek, CA 94596.

Note. This manuscript was submitted on September 10, 2018; approved on July 31, 2019; published online on October 25, 2019. Discussion period open until March 25, 2020; separate discussions must be submitted for individual papers. This paper is part of the ***Journal of Geotechnical and Geoenvironmental Engineering***, © ASCE, ISSN 1090-0241.

liquefaction. NDAs can provide an improved basis for estimating deformations over simplified methods that either do not account for the soil's constitutive response or are limited to idealized geometries and/or conditions. This becomes increasingly important in the performance-based evaluation of liquefaction consequences on structures. Still, the quality of results from an NDA study depends—amongst numerous factors (Boulanger and Ziotopoulou 2018; Tasiopoulou et al. 2019; Ziotopoulou et al. 2019)—on the selection and calibration of the constitutive model. As such, confidence in NDA results depends on the ability of the selected constitutive model(s) to do the following: (1) represent at the soil element level the loading responses important to the problem being analyzed; and (2) capture important mechanisms and reproduce known system responses (i.e., validation through large scale tests and/or case histories).

In the performance-based evaluation of liquefaction effects on soil and soil-structure systems, a well-calibrated constitutive model should at a minimum be able to capture two main aspects of the liquefaction problem: triggering and postliquefaction deformations. Even though there are multiple empirical correlations for estimating the cyclic resistance of sand-like materials (Seed and Idriss 1982; Idriss 1990; Andrus and Stokoe 1997; Idriss and Boulanger 2008; Boulanger and Idriss 2014) that provide a basis for model calibration in the absence of site-specific data, there is no equivalent quantitative framework for estimating post-triggering deformations. The latter may often be equally as important as the former in predicting liquefaction-induced deformations, particularly at sites subjected to large magnitude earthquakes, where the soils may liquefy early in the event and, subsequently, be subjected to many cycles of loading after liquefaction is triggered.

Research efforts have focused on interpreting the mechanisms of postliquefaction shear strain development based on laboratory experiments on sands (Shamoto et al. 1997; Zhang and Wang 2012) in attempts to provide mechanistic frameworks for quantitative evaluations. The common conclusion is that postliquefaction strains increase with the number of loading cycles (N_{cyc}). This interpretation has contributed to improved constitutive model formulations capable of the following: (1) accumulating strains in the post-triggering phase (versus locking up); and (2) predicting large postliquefaction shear strain development (e.g., Beaty and Byrne 1998; Yang et al. 2003; Tasiopoulou and Gerolymos 2016; Boulanger and Ziotopoulou 2017; Khosravifar et al. 2018). Currently, there are selected advanced constitutive models capable of replicating this behavior (e.g., PDMY02 and 03, PM4Sand, Ta-Ger, UBCSAND), but there is no framework available to guide their calibration for cases in which the postliquefaction triggering accumulation of shear strains at the element level and, by extension, displacements at the system level are important. Thus, so far, the common practice is to select individual experiments, when available, that can provide guidance on a case-by-case scenario via single-element numerical simulations. Giannakou et al. (2011) proposed a calibration methodology for postliquefaction shear strain accumulation targeting the maximum shear strain developed for 15 loading cycles at a range of cyclic stress ratios, *CSRs* and $N_{1,60}$ values, based on available direct simple shear laboratory tests. This methodology systematically accounted for postliquefaction shear strain development in the calibration process; however, no direct correlation with key parameters, such as *CSR* and $N_{1,60}$, was proposed. This methodology systematically targeted postliquefaction shear strain development in the calibration process; however, no direct correlation with key parameters, such as *CSR* and $N_{1,60}$, was proposed. Further systematic efforts to create a broader framework for calibration purposes were not readily identified in the literature.

The goal of this paper is to develop a framework for estimating the deformation (or shear strain) induced during the postliquefaction triggering phase in sands undergoing cyclic loading—already defined, herein, as postliquefaction deformation (or postliquefaction strain, respectively). This is done by the following: (1) collecting and investigating the range of demonstrated behaviors (i.e., accumulation of postliquefaction shear strains) as evidenced from cyclic undrained stress-controlled tests on clean sands under a range of conditions (relative densities D_R and overburden stresses σ'_{vc}); (2) developing a metric for the accumulation of postliquefaction strains; (3) using the proposed framework in the calibration methodology of an advanced constitutive model capable of capturing postliquefaction strain accumulation; and (4) validating the proposed framework through the simulation of two centrifuge tests, where significant shaking took place after liquefaction triggering.

Shear Strain Accumulation

Liquefaction-induced ground failure and deformation is frequently observed in earthquakes and is one of the most damaging effects of earthquake-induced soil liquefaction (e.g., Hamada and O'Rourke 1992; Cubrinovski et al. 2011; Yen et al. 2011; Tokimatsu et al. 2012). More specifically, liquefaction-induced shear-deformation has long been recognized as dependent on the dilation of the soil-skeleton, which leads to a transient increase in strength (Seed and Lee 1966; Casagrande 1976; Castro 1975; Castro and Poulos 1977; Seed 1979; Elgamal et al. 1998). Complications arising from the existence of sloping ground (static shear stress bias, α) have also received significant attention (Sivathayalan and Ha 2011; Chiaro et al. 2012).

Postliquefaction shear strain accumulation has been studied in laboratories through undrained cyclic tests on clean sands (Fig. 1) and sands with nonplastic fines (e.g., Seed and Lee 1966; Lee and Schofield 1988; Tatsuoka and Ishihara 1973; Ishihara 1985; Tatsuoka et al. 1986; Shamoto et al. 1997; Hatanaka et al. 1997). These studies have emphasized the increase in shear stiffness and strength during dilation at large shear strains along with an associated increase in confinement. However, the deformation of sand (e.g., Arulmoli et al. 1992; Kutter et al. 1994; Wahyudi 2014; Zhang et al. 1997) during the postliquefaction stage (initial liquefaction refers to the first occurrence of soil liquefaction, i.e., single amplitude shear strain of ~3% during cyclic loading) has predominantly received a qualitative rather than a quantitative interpretation with most of the efforts focusing on the ability of constitutive models to reproduce postliquefaction strains as a behavior but not on their ability to predict its magnitude (e.g., Yang et al. 2003; Kramer and Arduino 1999). This poses a significant constraint to the development of numerical predictive frameworks (e.g., constitutive models), which lack a calibration basis for their ability to predict postliquefaction strains particularly in the absence of site-specific laboratory experiments.

Significant shear strain is generated within each postliquefaction cycle, as conceptually illustrated in Figs. 2(a and b). Shear strains have been decoupled by Zhang and Wang (2012) into the postliquefaction shear strain at near-zero effective stress, denoted by γ_0 and the postliquefaction *dilation* strain, γ_d, occurring as the stress path follows the critical state line to reach the targeted shear stress. As shown in Fig. 2(a), significant deformation occurs at low effective stresses (between Points 1 and 2). Under uniform stress-controlled loading (constant *CSR*), γ_0 is systematically observed to increase as the cyclic loading continues, while γ_d obtains its maximum value at liquefaction triggering and remains practically constant in the postliquefaction stage (Zhang and Wang 2012).

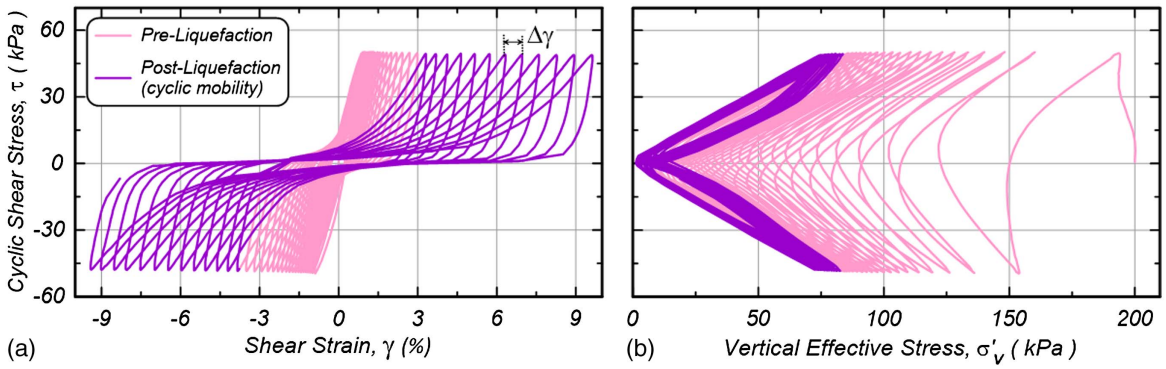

Fig. 1. Stress strain loops and effective stress path results for an undrained cyclic direct simple shear test on Fraser River sand pluviated at $D_R = 81\%$, subjected to a $CSR = 0.25$ and $\sigma'_{vc} = 200$ kPa. (Data from Sriskandakumar 2004.)

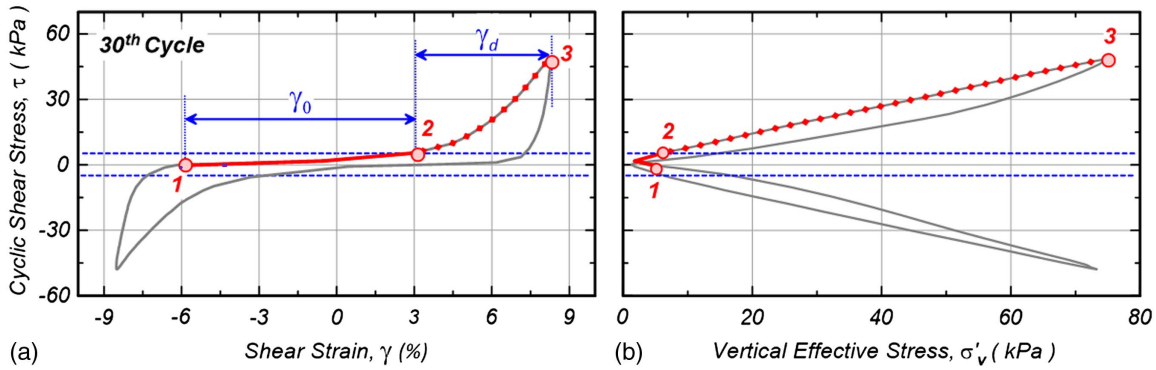

Fig. 2. (a) Isolated stress strain loop of 30th loading cycle; and (b) corresponding effective stress path of the test in Fig. 1.

The large postliquefaction shear deformation of sands and its progressive development have been observed in numerous undrained cyclic laboratory experiments (e.g., Chiaro et al. 2009; Wahyudi 2014; Zhang et al. 1997) and discrete element method (DEM) simulations (e.g., Wang et al. 2016; Wei and Wang 2017). Several constitutive model studies have employed heuristic assumptions that associate γ_0 with loading and fabric history (e.g., Elgamal et al. 2003; Zhang and Wang 2012; Wang et al. 2016; Boulanger and Ziotopoulou 2017) and some research groups (e.g., Wang et al. 2016) have developed new void-based fabric metrics that provide correlations to γ_0. Such metrics are impractical for most engineering applications because all experimental measurements provide only global-scale measurements of liquefaction-related behaviors (state, stress, strain, and pore pressure), and DEM modeling has not yet found a cost-efficient pathway to practice. As a result, little progress has been made toward providing guidance on the magnitude of deformation that liquefied sands will develop in the postliquefaction phase of their response.

Semiempirical Postliquefaction Shear Strain Accumulation Curves Based on Experimental Data

The progressive postliquefaction strain accumulation is difficult, if not impossible, to capture from case histories mainly because at the system level, the final response is governed by both stratigraphy and the boundary conditions of the system (e.g., free face and sloping ground). However, these responses can be reliably discerned in high-quality laboratory test results on clean sands once a proper methodology is adopted to extract and isolate the strains developed in the postliquefaction regime. This section describes the procedure developed to extract strain accumulation data from cyclic undrained stress-controlled laboratory experiments on clean sands.

Numerous researchers have contributed high-quality laboratory tests on clean sands. A broad range of cyclic undrained or equivalent-undrained constant volume stress-controlled tests on clean sands under level ground conditions (i.e., no initial static bias) was collected and summarized. Selection criteria for the collected tests included the following:

- Loading up to and beyond the triggering of liquefaction defined through a shear strain-based criterion. As far as possible, tests that reached liquefaction and provided a number of full cycles beyond that point were targeted so that a metric of the strain increment per cycle could be reliably measured. The minimum required number of cycles was considered to be four for sands with a D_R greater than ~40% and two for looser sands because they tend to develop large postliquefaction strains early on, with associated loss of constant stress control during the test;
- Tests that produced near-symmetric loops. This is a criterion that does not have a metric assigned to it. The authors relied on their experience with evaluating the quality of testing and on personal communication with the researchers when possible (S. Sriskandakumar, personal communication, 2017), recognizing that symmetry is almost impossible to perfectly attain in lab testing. This is consistent with the common understanding of cyclic behavior of sands. When a sand sample is sheared in one direction, especially under constant volume conditions, the effective vertical stress changes in a way that depends on the initial K_0-conditions and fabric related to the soil skeleton.

Thus, there is no reason it should produce the same level of strain when it is sheared in the opposite direction, even under the same cyclic shear stress;
- Tests that maintained a constant cyclic shear stress amplitude; and
- Tests accompanied by a detailed description of the experimental protocol followed in their execution. This facilitated confidence in the quality of the results.

The following subsection describes the processing of one set of laboratory tests.

Experimental Observations on Fraser River Sand

The high-quality experimental data presented in this subsection are results of cyclic undrained direct simple shear (DSS) tests performed at the University of British Columbia (Sriskandakumar 2004) on Fraser River sand under level ground conditions. The sand specimens were prepared by air pluviation for a range of relative densities (D_R = 31%–82%) and subjected to uniform stress-controlled loading under a wide range of cyclic stress ratios (CSR = 0.13–0.45) and initial vertical effective stresses (σ'_{vc} = 50–200 kPa). This database contains 25 tests.

Description and Processing of a Typical Test

Fig. 1 illustrates one undrained cyclic stress-controlled DSS test on air pluviated Fraser River sand at $D_R = 81\%$. The specimen liquefies and undergoes a continuous development of postliquefaction shear strains in the postliquefaction regime. Figs. 3(a and b) illustrate the shear strain amplitude (envelope of maximum shear strains) versus the number of cycles for this test. Herein and for the remainder of this paper, liquefaction triggering is defined as the state when the following conditions have occurred: (1) significant decrease of initial effective stress (i.e., corresponding to excess pore pressure ratio, $r_u > 0.7$); and (2) development of 3% single amplitude (SA) shear strain. For the test illustrated in Fig. 1, liquefaction triggering takes place after 20 cycles of loading, followed by 12 cycles of loading in the postliquefaction stage. The rate of shear strain accumulation continuously increases until it reaches a maximum (or saturation) value in the postliquefaction stage. This behavior has been also hypothesized and validated by Wang et al. (2016) and Zhang and Wang (2012). The rate of shear strain accumulation is defined as the difference in shear strain amplitude, either single or double, between two consecutive cycles, and is herein denoted as $\Delta\gamma$. Fig. 3(c) illustrates $\Delta\gamma$ plotted versus the number of cycles and demonstrates the aforementioned trend of gradual postliquefaction increase until a plateau is reached. The postliquefaction shear strain ($\gamma_{postliq}$) is defined

$$\gamma_{postliq} = \gamma_{DA/2} - \gamma_{liq(3\%)} \tag{1}$$

where $\gamma_{DA/2} (= \gamma_{DA}/2)$ = average SA shear strain, estimated as half of the DA shear strain; and γ_{liq} = approximately 3%. These extracted values are plotted versus the number of cycles in the postliquefaction stage, $N_{cyc,postliq}$, which starts counting at liquefaction triggering ($N_{cyc,postliq} = N_{cyc} - N_{cyc,liq}$). Fig. 3(d), indicates an almost linear increase of postliquefaction shear strain

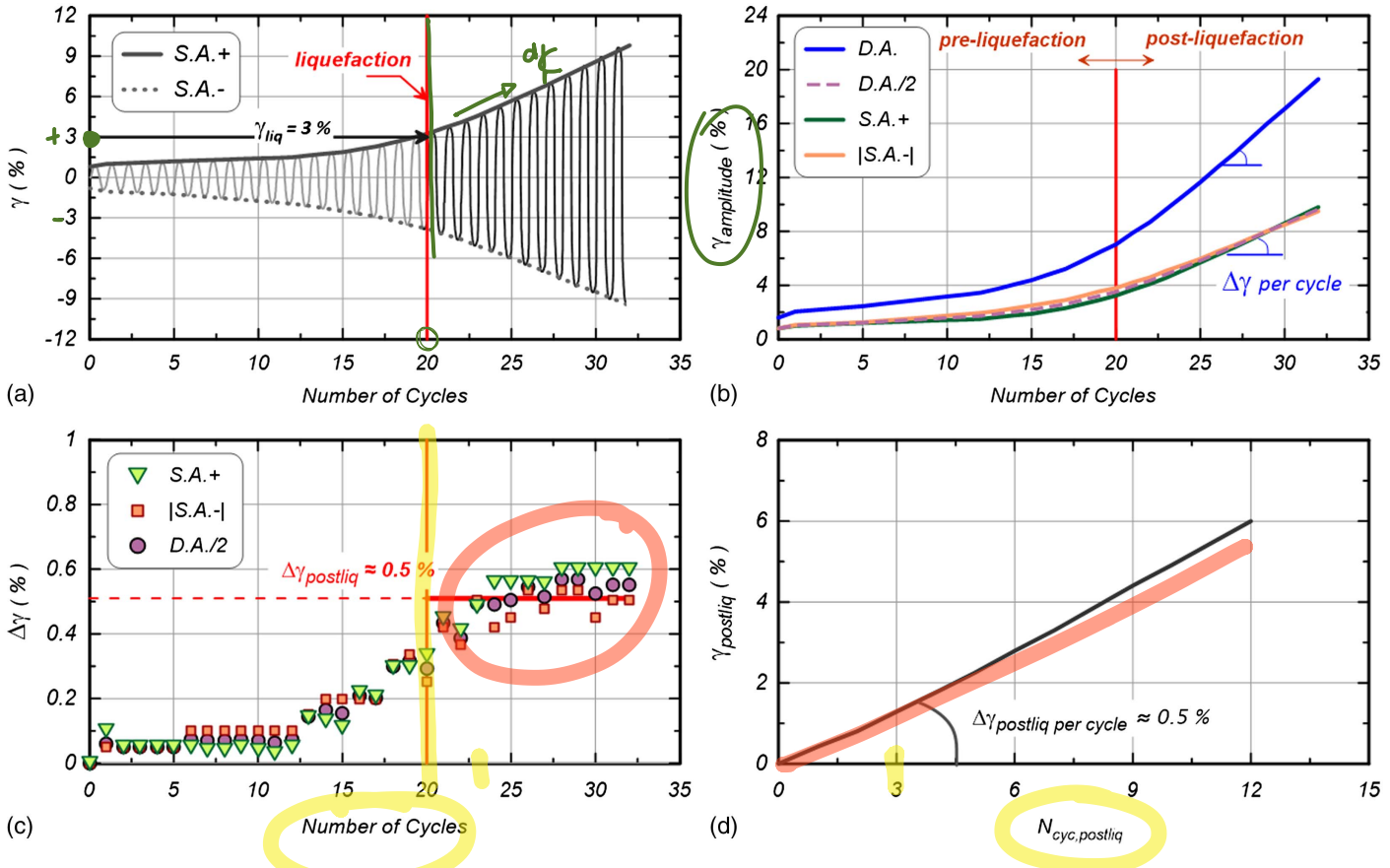

Fig. 3. (a) Stress strain versus number of loading cycles; (b) envelope of single amplitude (SA) and double amplitude (DA) shear strains versus number of loading cycles; (c) rate of shear strain accumulation, defined as the difference of shear strain amplitude, either SA or DA, between two consecutive cycles, $\Delta\gamma$, versus number of loading cycles; and (d) postliquefaction shear strains versus postliquefaction number of loading cycles. All plots refer to laboratory test in Fig. 1.

J. Geotech. Geoenviron. Eng., 2020, 146(1): 04019120

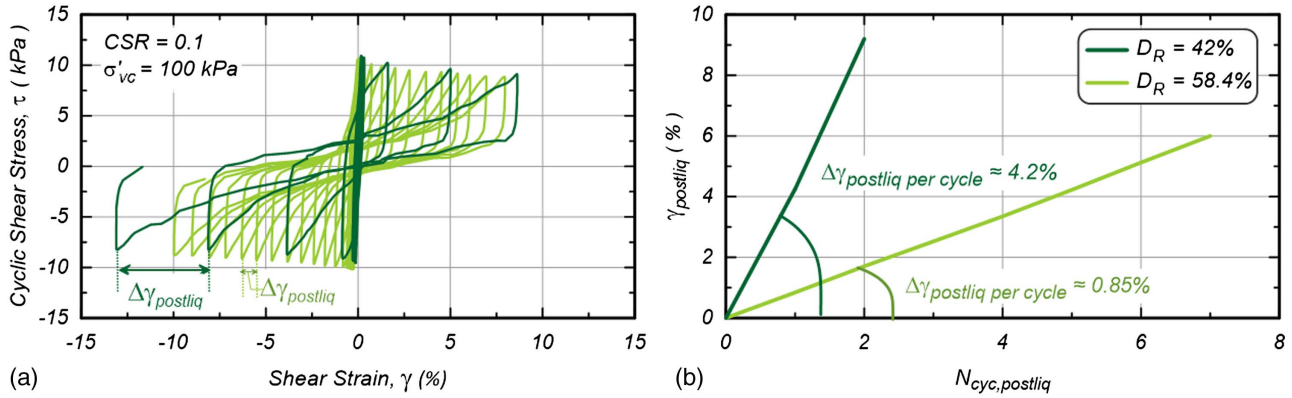

Fig. 4. Stress strain loops and postliquefaction shear strains versus postliquefaction number of loading cycles for two undrained DSS tests on Fraser River sand with $D_R = 42\%$ and 58.4%. (Data from Sriskandakumar 2004.)

versus $N_{cyc,postliq}$, suggesting a constant value of $\Delta\gamma$, herein termed as $\Delta\gamma_{postliq}$ *per cycle*, equal to approximately 0.5% for this experiment.

Similar processing was performed on the 25 experiments conducted by the same group of researchers on Fraser River sand. Upon reviewing the results, a systematic trend was identified in that a nearly constant rate, $\Delta\gamma_{postliq}$ *per cycle*, seemed characteristic of the postliquefaction stage in all of the tests. This rate was selected as a metric of postliquefaction shear strain accumulation because of the following: (1) it can be conveniently measured in the lab; and (2) it can be practically applied to estimate shear strain accumulation, once liquefaction triggering and the number of loading cycles in the postliquefaction stage are known, as follows:

$$\gamma = \gamma_{liq(3\%)} + N_{cyc,postliq} \cdot \Delta\gamma_{postliq}\, per\, cycle \qquad (2)$$

Dependency of $\Delta\gamma_{postliq}$ *per Cycle* on D_R

As a first step in the development of semiempirical postliquefaction shear strain relationships from experimental data, the critical parameters affecting postliquefaction shear strain accumulation were identified. Commonly, the likelihood of triggering liquefaction was estimated by comparing cyclic resistance, dependent on D_R and the initial effective stress σ'_{vc} (or their combined state—Been and Jefferies 1985), with the cyclic demand or *CSR*. This has led to the development of liquefaction resistance curves, expressed in terms of *CSR* versus N_{cyc}, varying with D_R and initial effective stress (Seed and Idriss 1982; Andrus and Stokoe 1997; Idriss and Boulanger 2008; Boulanger and Idriss 2014). Given the importance of D_R to liquefaction triggering, it seemed reasonable to expect that this parameter is also important to postliquefaction shear strain accumulation. To investigate this assumption, two experiments with different D_R's (42% and 58.4%) and loaded with the same *CSR* under the same initial vertical effective stress ($\sigma'_{vc} = 100$ kPa), were compared and are illustrated in Fig. 4 using the process previously described. As shown in this figure, the $\Delta\gamma_{postliq}$ *per cycle* is about five times larger for the looser ($D_R = 42\%$) sample than for the denser ($D_R = 58.4\%$) one. The strong dependence of $\Delta\gamma_{postliq}$ *per cycle* on D_R is better demonstrated on the semilogarithmic plot of Fig. 5, which presents data from the 25 experiments on Fraser River sand (Sriskandakumar 2004). As D_R increases from 40% to 80%, postliquefaction shear strain rates decrease by about two orders of magnitude. The experimental data clearly indicate that D_R is a critical parameter affecting the postliquefaction shear strain rate, a finding also identified previously by De Alba et al. (1976). However, as seen in Fig. 5, the scatter in these data is significant and does not allow for the development of a well-constrained correlation between $\Delta\gamma_{postliq}$ *per cycle* and D_R.

Dimensional Analysis of $\Delta\gamma_{postliq}$ *per Cycle* and D_R

In order to develop a metric to both (1) capture postliquefaction shear strain accumulation, and (2) provide a reasonable correlation with D_R, the next step was to develop a normalized plot of $\Delta\gamma_{postliq}$ *per cycle* versus D_R. Because liquefaction triggering of sand is primarily associated with *CSR* and the initial effective stress σ'_{vc}, these parameters were initially considered appropriate candidates for the normalization of $\Delta\gamma_{postliq}$ *per cycle*. To evaluate their effect on postliquefaction sand behavior, two experiments on Fraser River sand with the same $D_R = 80\%$ and $CSR = 0.3$, but tested under different σ'_{vc} values (100 and 200 kPa, respectively) leading to different cyclic shear stress amplitudes τ_{cyc} (30 and 60 kPa, respectively), were compared and are illustrated in Fig. 6. The first four graphs in the figure [Figs. 6(a–d)] compare these two experiments in terms of stress-strain loops, stress paths, and shear strain versus number of loading cycles. The following observations are drawn: (1) as expected, fewer cycles are required for liquefaction triggering (3% SA shear strain) with increasing σ'_{vc} because the sand becomes less dilative and reaches liquefaction faster; and (2) the rate of

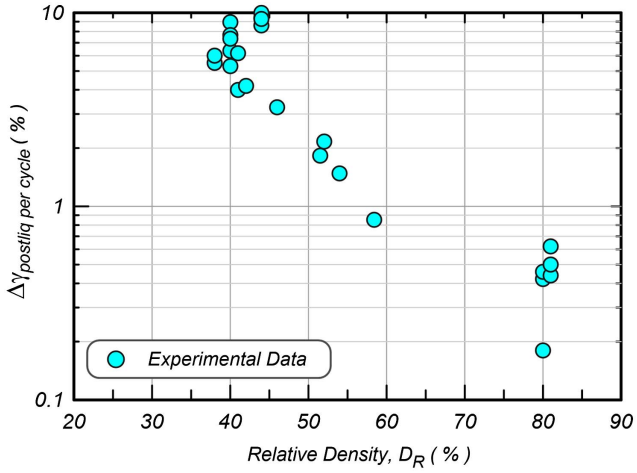

Fig. 5. Postliquefaction shear strain rate, $\Delta\gamma_{postliq}$ *per cycle* versus D_R, for 25 undrained DSS tests on Fraser River sand.

J. Geotech. Geoenviron. Eng., 2020, 146(1): 04019120

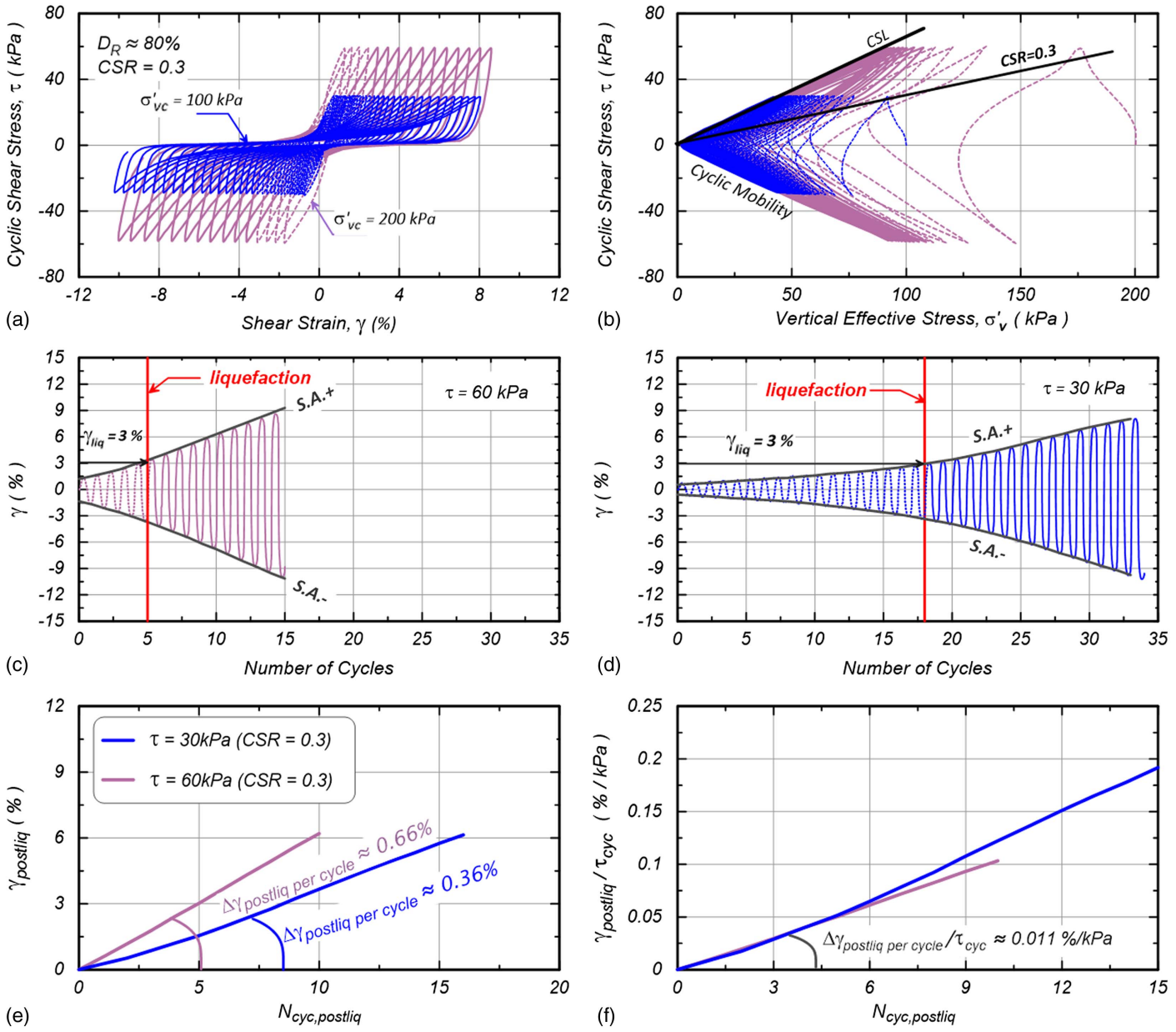

Fig. 6. Comparison of undrained DSS tests on Fraser River sand samples with $D_R = 80\%$, $CSR = 0.3$, and different initial effective stress ($\sigma'_{vc} = 100$ and 200 kPa), resulting in different shear stress amplitude ($\tau_{cyc} = 30$ and 60 kPa): (a) stress-strain loops; (b) effective stress paths; (c) stress-strain versus number of loading cycles for the test with $\tau_{cyc} = 60$ kPa; (d) stress-strain versus number of loading cycles for the test with $\tau_{cyc} = 30$ kPa; (e) postliquefaction shear strains, $\Delta\gamma$, versus number of loading cycles; and (f) postliquefaction compliance rate, $\Delta\gamma_{postliq}/\tau_{cyc}$, versus number of loading cycles.

postliquefaction shear strain accumulation ($\Delta\gamma_{postliq}$ *per cycle*) for a given *CSR* increases with increasing σ'_{vc} and, thus, with increasing τ_{cyc}.

Sand behavior is effective-stress dependent and, as such, liquefaction triggering is commonly linked with *CSR* rather than the cyclic shear stress amplitude, τ_{cyc}. *CSR* provides a metric of the distance between the initial stress ratio state and the critical stress ratio [at the critical state line (*CSL*)], which can be a measure of liquefaction resistance [Fig. 6(b)]. It is thus reasonable to consider whether *CSR* is equally important in the postliquefaction regime or not. The development of postliquefaction shear strains occurs after liquefaction initiation once the critical stress ratio is reached (Zhang et al. 1997) and progressive contractions and dilations take over, leading the stress state to dive into the origin and climb back up the failure envelope, respectively [Fig. 6(b)]. This is accompanied by the development of strains [see also Fig. 2(b)]. Considering the responses illustrated in Fig. 6 in conjunction with Fig. 2, the conclusion can be drawn that the development of postliquefaction shear strains under uniform loading should be related to the magnitude of shear stress. The comparison between the two experiments in terms of postliquefaction shear strains versus $N_{cyc,postliq}$ in Fig. 6(e) demonstrates that the $\Delta\gamma_{postliq}$ *per cycle* for $\tau_{cyc} = 60$ kPa is almost double that for $\tau_{cyc} = 30$ kPa. Attempting to normalize $\gamma_{postliq}$ in Fig. 6(e) with *CSR* would produce the same trend, whereas normalizing $\gamma_{postliq}$ with shear stress amplitude, τ_{cyc}, [Fig. 6(f)] results in near-identical normalized rates of shear strain accumulation per cycle. Based on the experimental data and the fundamental understanding of the element response, τ_{cyc} stood out as a more

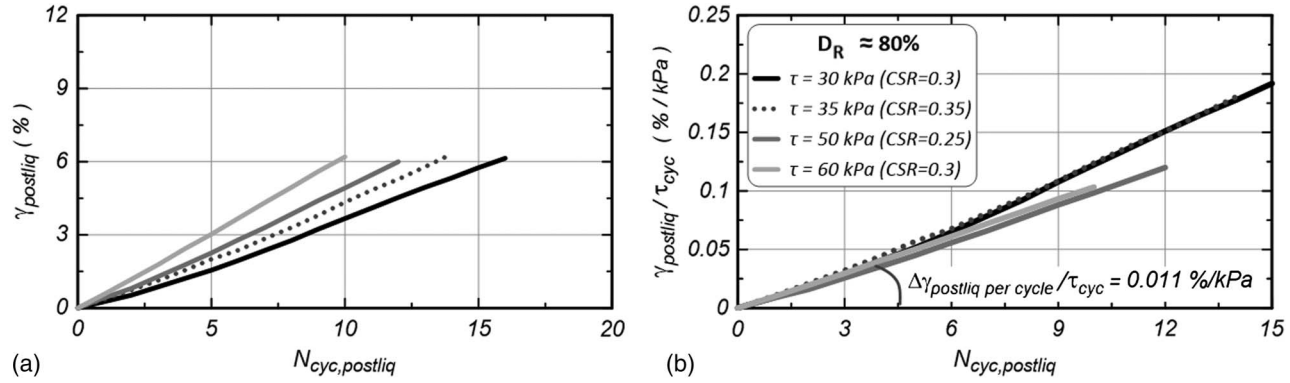

Fig. 7. (a) Postliquefaction shear strains; and (b) normalized postliquefaction shear strains versus postliquefaction number of loading cycles for four different undrained DSS tests on Fraser River sand with $D_R = 80\%$.

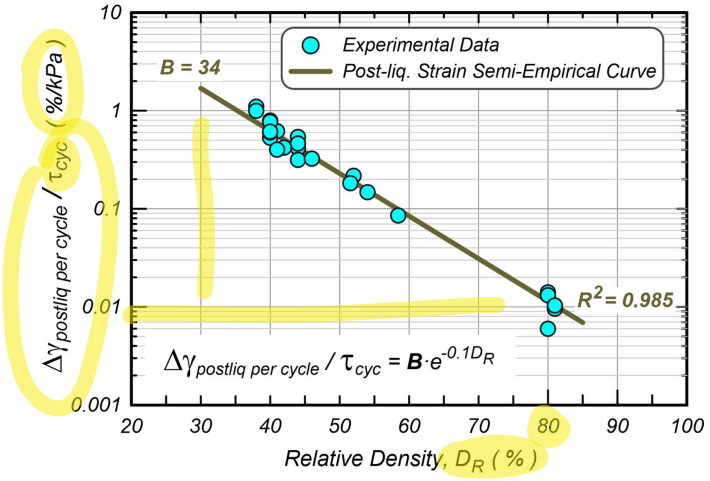

Fig. 8. Postliquefaction compliance rate, $\Delta\gamma_{postliq}\ per\ cycle/\tau_{cyc}$ versus D_R, for 25 undrained DSS tests on Fraser River sand and development of semiempirical postliquefaction shear strain curve.

appropriate parameter to normalize the shear strain accumulation per cycle.

To check the suitability of the normalization with τ_{cyc}, experiments on specimens with the same $D_R = 80\%$ and varying amplitudes of τ_{cyc} (or CSR and σ'_{vc}) were selected. The process was described previously and is illustrated in Fig. 7(a). The normalization of $\gamma_{postliq}$ with τ_{cyc}, shown in Fig. 7(b), led to a reduction in the obtained scatter and allows for the reasonable assumption of a common value for $\Delta\gamma_{postliq}\ per\ cycle/\tau_{cyc}$ for a given D_R.

The normalized parameter $\Delta\gamma_{postliq}\ per\ cycle\ /\tau_{cyc}$ is a measure of compliance (i.e., inverse of stiffness). A physical context to this parameter is provided in Fig. 7(b): the vertical axis represents the inverse of a postliquefaction secant shear modulus, which increases linearly with the number of cycles N_{cyc}, implying a decrease of stiffness (increase of compliance) indicative of a gradual material softening. Thus, $\Delta\gamma_{postliq}\ per\ cycle\ /\tau_{cyc}$ represents the rate of increase of compliance with an increasing number of loading cycles and hereafter is referred to as the compliance rate.

Compilation of All Tests

Normalization of the postliquefaction shear strain rate per cycle with shear stress amplitude, τ_{cyc}, for all 25 experiments on Fraser River sand yielded a better correlation versus D_R, as illustrated in Fig. 8. Compared to Fig. 5, the normalization with τ_{cyc} reduced the scatter of the data, allowing for the development of a semiempirical power relationship between the compliance rate, $\Delta\gamma_{postliq}\ per\ cycle/\tau_{cyc}$, and D_R using a linear least square fitting method

$$\Delta\gamma_{postliq}\ per\ cycle/\tau_{cyc} = B \cdot e^{A \cdot D_R} \tag{3}$$

where $B = 34$ and $A = -0.1$ for $R^2 = 0.99$. Eq. (3) and by extension the values for A and B are valid when the units of $\Delta\gamma_{postliq}\ per\ cycle$, τ_{cyc}, and D_R are %, kPa and % respectively.

To evaluate whether this trend can be generalized for liquefiable sands and to investigate whether this function can describe the postliquefaction shear strain accumulation of other sands, additional data were examined and are subsequently described.

Extending the Database to More Laboratory Tests on Sands

The processing procedure outlined in section "Experimental Observations on Fraser River Sand" was applied to the databases of four more types of laboratory sands summarized in Table 1 (91 laboratory tests in total). During this process, it was observed that, much like the Fraser river tests, the majority of the tests exhibited a practically linear accumulation of the postliquefaction shear strains with the number of cycles, implying a constant compliance rate. A few tests (15 out of 91) showed some deviation from a constant compliance rate, either exhibiting a decreasing rate or an increasing rate or both with an increasing number of cycles. Rather than discarding this fraction of the sample set, an upper bound constant compliance rate was selected for these tests. While there is research work that indicates a decrease of the rate (e.g., Shamoto et al. 1997; Zhang and Wang 2012) or saturation (e.g., Wang et al. 2016) at certain strain thresholds or after a certain number of loading cycles, those studies were either based on individual tests or DEM simulations. The current study evaluated postliquefaction behavior from a large database of laboratory undrained cyclic tests and found that the use of a constant compliance rate was a rational approach for practical engineering purposes.

Semiempirical curves were developed for the four additional types of sand using the functional form of Eq. (3). Notably, a similar trend was identified for each of the sand types examined, allowing for the use of a common slope ($A = -0.1$) for all sands and adjusting only the B value [Eq. (3)]. Fig. 9 illustrates the scatter of the experimental data of all five types of sand along with the semiempirical fits to the data. Table 2 summarizes the

J. Geotech. Geoenviron. Eng., 2020, 146(1): 04019120

Table 1. List of experimental data used

Types of sand	Number of tests	D_R (%)	σ'_{vc} (kPa)	CSR	References
Monterey	26	31–82	77–95	0.1–0.3	Wu (2002)
Fraser River	25	38–81	50–200	0.13–0.45	Sriskandakumar (2004)
Nevada	12	37–90	33–98	0.04–0.48	Kammerer et al. (2000), Arulmoli et al. (1992), and Ziotopoulou (2016)
Ottawa F-65	12	42–77	100	0.08–0.22	Ziotopoulou et al. (2018) and Parra Bastidas (2016)
Toyoura	16	24–82	98–100[a]	0.16–0.40	Tatsuoka et al. (1986), Kiyota et al. (2008, 2010), Zhang and Wang (2012), Chiaro et al. (2012), De Silva et al. (2015), and Umar et al. (2016)

[a]Initial isotropic effective stress.

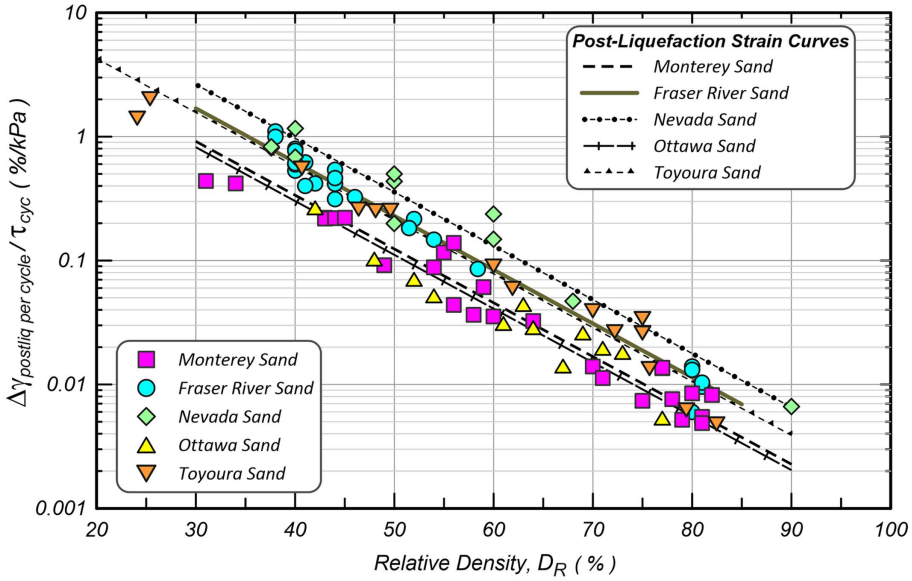

Fig. 9. Postliquefaction compliance rate, $\Delta\gamma_{postliq}\,per\,cycle/\tau_{cyc}$ versus D_R, for undrained stress-controlled tests on five types of sand and development of semiempirical postliquefaction shear strain curves for each type of sand.

Table 2. Sand characteristics, type of testing, and values of semiempirical postliquefaction shear strain equation parameters

Types of sand	D_{50} (mm)	C_u	Grain shape	Test	Sample preparation	B[a]	A[b]	R^2[c]
Monterey	0.36	1.2	Sub-rounded	DSS	Air pluviation	18.4	−0.1	0.95
Fraser River	0.26	1.6	Sub-angular	DSS	Air pluviation	34	−0.1	0.99
Nevada	0.14	1.4	Sub-rounded	DSS	Air pluviation	53	−0.1	0.96
Ottawa F-65	0.2	1.6	Sub-rounded to rounded	DSS	Air pluviation	16.5	−0.1	0.90
Toyoura	0.17	1.5	Angular to sub-angular	Hollow cylinder	Air pluviation	31.5	−0.1	0.96

[a]B value in prediction Eq. (3).
[b]A value (slope) in prediction Eq. (3).
[c]R^2 statistic error of semiempirical prediction curves.

characteristics of the sand materials, experimental details, and the B, A, and R^2 values of all the power fits.

The limited experimental data for very loose sands (e.g., only Monterey and Toyoura sand datasets included data with $D_R < \sim 35\%$), combined with the difficulty in maintaining stress control for an adequate number of cycles (>2 or 3) after liquefaction triggering, may limit the applicability of the semiempirical curves to a range of D_R between 35%–40% and 80%. However, the applicable range does cover the vast majority of earthquake engineering applications in which the developed framework would play a role.

The developed semiempirical curves were based on laboratory tests under a constant cyclic shear stress amplitude. Tests with varying amplitudes in the postliquefaction regime have shown that the postliquefaction shear strain accumulation depends on the current shear stress (Sento and Shimazaki 2013). The developed framework can be applied to earthquake loading by using compliance rates dependent on the current shear stress over each cycle after liquefaction is triggered.

Statistical Evaluation of the Collected Experimental Database

Linear regression using a least square criterion was performed on the cumulative body of experimental data obtained for a range of sands. The regression considered the functional form of Eq. (4) obtained from Eq. (3)

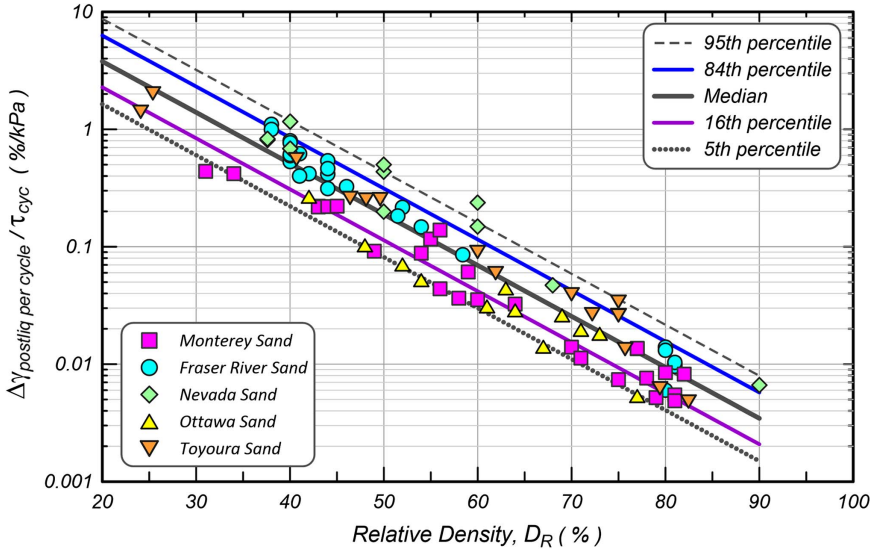

Fig. 10. Generic postliquefaction shear strain curves corresponding to the median curve together with the 5th, 16th, 84th, and 95th percentiles, obtained from linear regression of the whole body of experimental data.

$$\ln(\Delta\gamma_{postliq}\ per\ cycle/\tau_{cyc}) = A \cdot D_R + \ln(B) \quad (4)$$

The compliance rate correlation derived from statistical evaluation can be expressed

$$\Delta\gamma_{postliq}\ per\ cycle/\tau_{cyc} = \exp(A \cdot D_R + \ln(B_{50\%}) + \varepsilon_{\ln(\cdot)}) \quad (5)$$

where $\varepsilon_{\ln(\cdot)}$ is normally distributed with a mean of 0 and a standard deviation of $\sigma_{\ln(\cdot)} = 0.5$; and $B_{50\%} = 28$. Because the variation in the slope term was minimal, a deterministic slope ($A = -0.1$) was adopted. Fig. 10 illustrates the median curve together with the 5th, 16th, 84th, and 95th percentile relationships.

The goal of the statistical evaluation of the collected experimental database is to provide a general estimate of the rate of postliquefaction shear strain accumulation and the associated uncertainty. Because the database has considered a number of different siliceous sands, these relationships can be used to estimate the postliquefaction shear stains in the absence of soil-specific test data. Undoubtedly, the availability of site-specific data would reduce the uncertainty in the preceding described statistical estimates.

The semiempirical relationship described by Eq. (5) and illustrated in Fig. 10 is intended to be used in conjunction with liquefaction resistance curves for the appropriate calibration of constitutive models and the subsequent reliable evaluation of soil and soil-structure system deformations in effective stress NDAs. In the following sections, these relationships are utilized in the framework of an NDA using the PM4Sand constitutive model: a calibration methodology is introduced to capture both liquefaction triggering and postliquefaction shear strain accumulation followed by system-level numerical simulations of two centrifuge model experiments.

Constitutive Model Calibration Using the Semiempirical Framework: System Level Validation against Centrifuge Experiments

Two centrifuge model tests studying liquefaction-induced demands on two different soil-structure systems (i.e., an immersed tunnel and a quay wall) were selected to evaluate if calibrations using the preceding described framework leads to improved estimates of liquefaction-induced deformations. The two tests were simulated using a constitutive model calibrated for liquefaction triggering as well as postliquefaction shear strain accumulation based on the preceding framework described. The information provided in this section, in combination with the FLAC 8 manual (Itasca 2016), the PM4Sand manual (Version 3.1) (Ziotopoulou and Boulanger 2016; Boulanger and Ziotopoulou 2017), and the archived experimental data reports for the corresponding centrifuge model tests (Chou et al. 2008; Sato et al. 2001), are sufficient for recreating the analyses presented here. The following descriptions of the model parameters and numerical procedures assume familiarity with the aforementioned references.

The overarching goal of using the preceding relationships developed in the calibration process is to improve the reliability of performance estimates for foundations and geotechnical structures affected by liquefaction-induced soil deformation mechanisms. Thus, the criteria considered for selecting centrifuge model experiments were the following: (1) strong input motion that allowed for both liquefaction occurrence and postliquefaction deformation; and (2) soil-structure interaction. Considering the preceding criteria, two centrifuge experiments were selected from the literature, studying the performance of the following: (1) the BART offshore Transbay Tube that connects Oakland to San Francisco, California (Chou et al. 2011); and (2) a sheet pile quay wall with liquefiable backfill (Sato et al. 2001). The first experiment comprises two different types of laboratory sands, Nevada and Monterey sand, at three different relative densities ($D_R = 32\%$, 40%, and 50%) surrounding the model tunnel. The calibration of the PM4Sand constitutive model was based on liquefaction triggering and postliquefaction shear strain curves obtained from laboratory tests on these types of sand. The second experiment comprises a liquefiable backfill of Silica sand No. 8 with $D_R = 50\%$. Due to the lack of soil-specific experimental data for this type of sand (a common occurrence in engineering practice), calibration was based on generic empirical liquefaction resistance curves and the semiempirical postliquefaction shear strain curves presented in Fig. 10. The use of this generic calibration process provides insights into the range of applicability of the proposed semiempirical postliquefaction shear strain curves.

Liquefaction-Induced Uplift of Immersed Tunnel

The Offshore Transbay Tube (TBT) of the Bay Area Rapid Transit (BART) system is a 5.8 km-long immersed railway tunnel located in a region of high seismicity in San Francisco, California. Fugro assessed the vulnerability of the TBT to uplift resulting from liquefaction of the surrounding soils during the design earthquakes. To assist with the preceding goal, two centrifuge experiments were performed in 2007 at the large-scale centrifuge facility at the Center for Geotechnical Modeling (CGM) at the University of California, Davis. The numerical simulation presented in this paper was conducted for the JCC01 centrifuge model and the main shaking event *TCU*, which was a modified version of the TCU078 (CESMD 1999) record from the 1999 Chi-Chi Earthquake (Lee and Shin 2001) with a PGA = 0.65 g.

The centrifuge model of the TBT included the submerged tube, surrounded by liquefiable fill and foundation course (loose gravel under the tube), as depicted in Fig. 11 in a prototype scale. Monterey sand 0/30 was used to represent the loose gravel under the tube and the gravel that filled the prototype trench up to the tube spring line. Nevada sand was used to represent the loose sand that filled the trench and provided a minimum cover for the tube. A mini cone penetration test (CPT) was performed prior to the shaking events to provide estimates of the soil density in the trench. Interpreted CPT data indicated as-built relative densities of 32%, 50%, and 40% for the Nevada Sand, the Monterey Sand adjacent to the tunnel, and the Monterey Sand beneath the tunnel (foundation), respectively. The model was built within a rigid container box. More details on the centrifuge modeling are provided in Chou et al. (2011) and details on the numerical simulations performed at the time are described by Travasarou et al. (2011).

The numerical model constructed in FLAC 8 (Itasca 2016) is shown in Fig. 11. Beam structural elastic elements were used for the simulation of the tunnel, while frictional interfaces were used to allow slippage between the tunnel and the surrounding soil with an interface friction angle of 23°. The displacement was fixed at the vertical boundaries and at the base of the model where the input motion was applied to simulate the boundary conditions imposed by the rigid container. The surficial mud and stiff clay were modeled using the Itasca S3 hysteretic model (Itasca 2016) in combination with a Mohr-Coulomb failure criterion. The model parameters were fit to approximate target shear modulus reduction curves from Darendeli (2001) based on a plasticity index (PI) equal to 15. The undrained shear strength of the stiff clay was assumed to be ~140 kPa. Because an undrained strength is assigned to the clay materials, changes in pore pressure do not affect their strength. The coarse-grained materials were modeled using the PM4Sand model while the values of permeability assigned to the coarse grained fills were 0.075 cm/s for Nevada sand and 0.88 cm/s for Monterey sand as suggested by Chou et al. (2011).

Constitutive Model Calibration of Sand-Like Materials Using Soil-Specific Lab Data

The PM4Sand constitutive model was assigned to the Nevada and Monterey sand fills. PM4Sand is a stress-ratio controlled, critical-state compatible bounding-surface plasticity model, which follows the framework of the Dafalias and Manzari (2004) model. The model has 22 input parameters, from which only three are considered primary and are required as model input. These are the apparent relative density (D_{Ro}), the shear modulus coefficient (G_0) used to define the elastic shear modulus, and the contraction rate parameter (h_{p0}) used for calibration of the undrained cyclic shear strength. The other 19 can be either left with their preset default values, which are generally functions of an index property if no other information is available, or calibrated to the desired response based on the available lab data. Boulanger and Ziotopoulou (2017) provide a detailed discussion of the formulation of the model as well as its parameters.

Calibration of the model prioritized both liquefaction triggering and postliquefaction shear strain accumulation. Data from

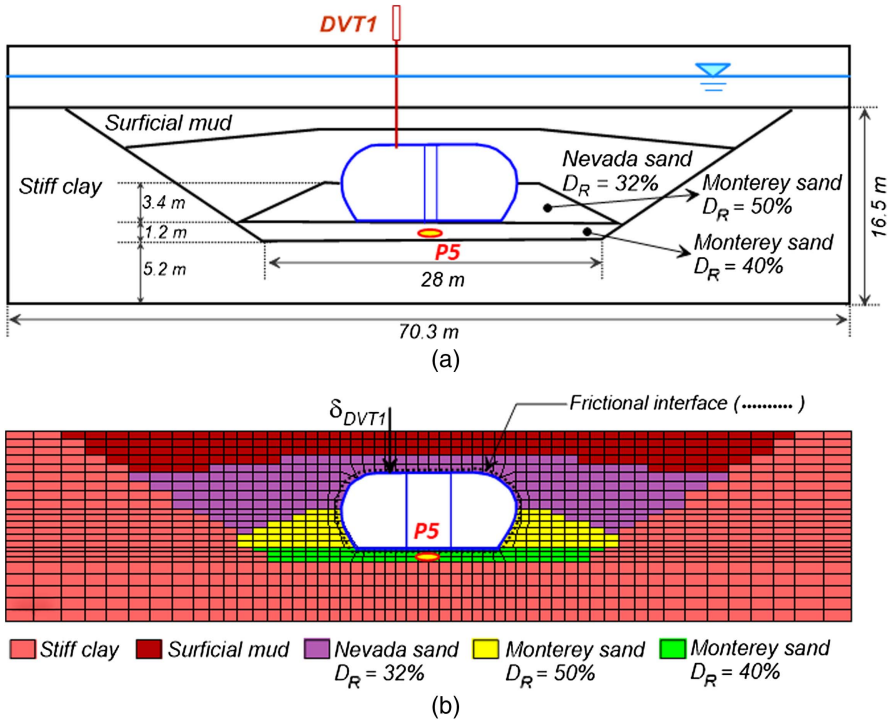

Fig. 11. (a) Centrifuge model; and (b) numerical model of the BART Transbay Tube in prototype scale.

J. Geotech. Geoenviron. Eng., 2020, 146(1): 04019120

Table 3. Model parameters for the numerical simulation of the BART centrifuge test

PM4Sand parameters	Nevada sand, $D_R = 32\%$	Monterey sand, $D_R = 40\%$	Monterey sand, $D_R = 50\%$
Primary			
D_{R0}	35%	40%	50%
G_0	Default[a]	Default[a]	Default[a]
h_{p0}	0.4	5	5.5
Secondary			
n^b	0.7	0.12	0.3
C_ε	500	Default	Default
z_{max}	100	Default	Default

[a]Calculated as $G_0 = 167\sqrt{(N_1)_{60} + 2.5} = 167\sqrt{46D_R^2 + 2.5}$ (Boulanger and Ziotopoulou 2017).

laboratory undrained direct simple shear tests, found in literature, on Nevada sand samples with $D_R = 40\%$ (Arulmoli et al. 1992; Doygun 2009; S. Kano personal communication, 2009) and Monterey sand samples with D_R varying from 35% to 60% (Kammerer et al. 2000; M. Riemer, personal communication, 2007) were used to calibrate liquefaction triggering behavior. Single element simulations using the PM4Sand model were performed within the calibration process to obtain model parameter values that reasonably match the processed experimental data for the following: (1) *CSR* versus number of cycles to liquefaction; and (2) postliquefaction compliance rate, $\Delta\gamma_{postliq}\, per\, cycle/\tau_{cyc}$, given by the semiempirical curves proposed in this study for Nevada and Monterey sand. Table 3 summarizes the calibrated model parameters. The apparent relative density D_{Ro}, the shear modulus coefficient G_0, and the contraction rate parameter h_{p0} are primary input parameters. The slope of the bounding line, and by extension triggering, as well as the rate of strain accumulation in the post-triggering phase of loading are controlled by the parameter n^b. The variable C_ε is also used to adjust the rate of strain accumulation in undrained cyclic loading. The variable z_{max} represents the maximum value the fabric tensor z can attain (Dafalias and Manzari 2004) and was also adjusted to control this aspect of the response. All other secondary parameters of PM4Sand are default values.

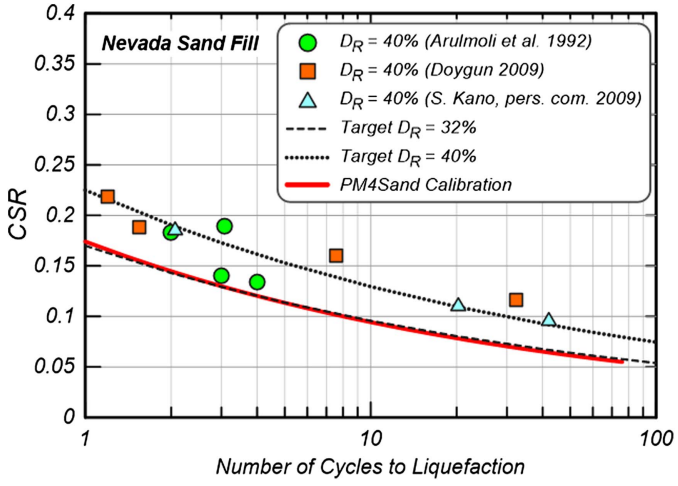

Fig. 12. Liquefaction resistance curve for Nevada ($D_R = 32\%$) sand fill obtained from PM4Sand single element simulations against experimental data.

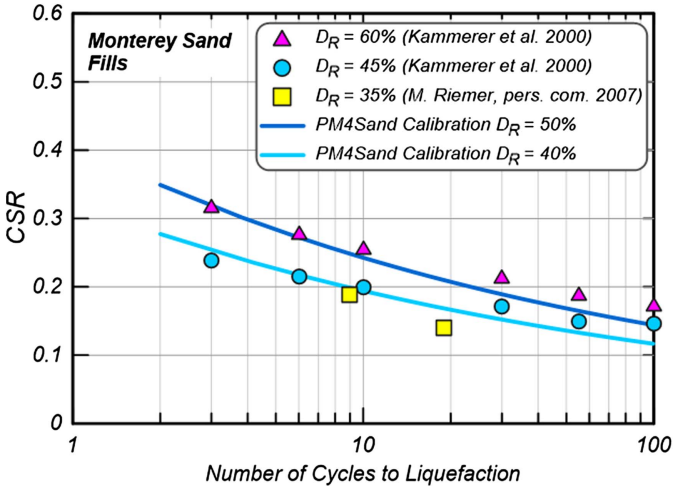

Fig. 13. Liquefaction resistance curves for Monterey sand fills ($D_R = 40\%$ and 50%) obtained from PM4Sand single element simulations against experimental data.

Figs. 12 and 13 depict the liquefaction resistance curves obtained by PM4Sand single element simulations versus experimental data. For Nevada sand, the target liquefaction resistance was taken as the lower bound of the available data due to the lack of experimental data on samples with $D_R = 32\%$ and the substantial scatter of the laboratory data on samples with $D_R = 40\%$. The postliquefaction compliance rates, $\Delta\gamma_{postliq}\, per\, cycle/\tau_{cyc}$, obtained from the single element simulations under different *CSRs* using PM4Sand are compared with the semiempirical curves for Nevada and Monterey sand in Fig. 14. It should be mentioned that both liquefaction triggering and postliquefaction shear strain accumulation were achieved with a single set of model parameters, specific for each D_R, as shown in Table 3. Fig. 15 depicts a comparison between single element simulation (continuous line) and laboratory data from Wu (2002) (dotted line) under undrained DSS loading conditions for Monterey sand with $D_R = 44\%$. The single element simulation was performed using the model parameter shown in Table 3 for Monterey sand with $D_R = 40\%$, apart from

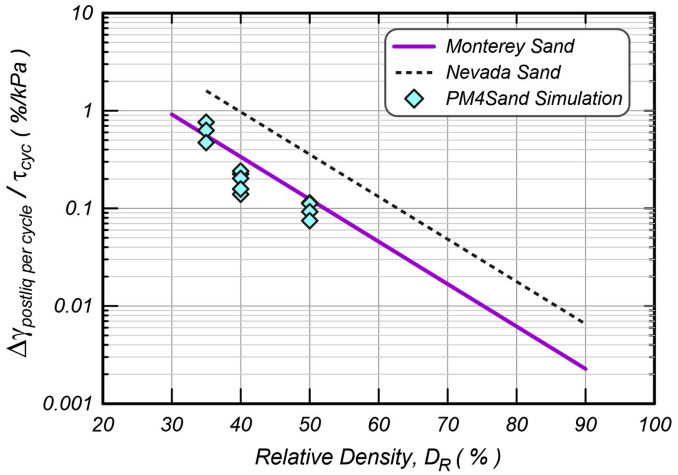

Fig. 14. Postliquefaction compliance rate for Nevada ($D_R = 35\%$) and Monterey ($D_R = 40\%$ and 50%) sand fills obtained from PM4Sand single element simulations (ran under different *CSRs* at each D_R) against semiempirical curves.

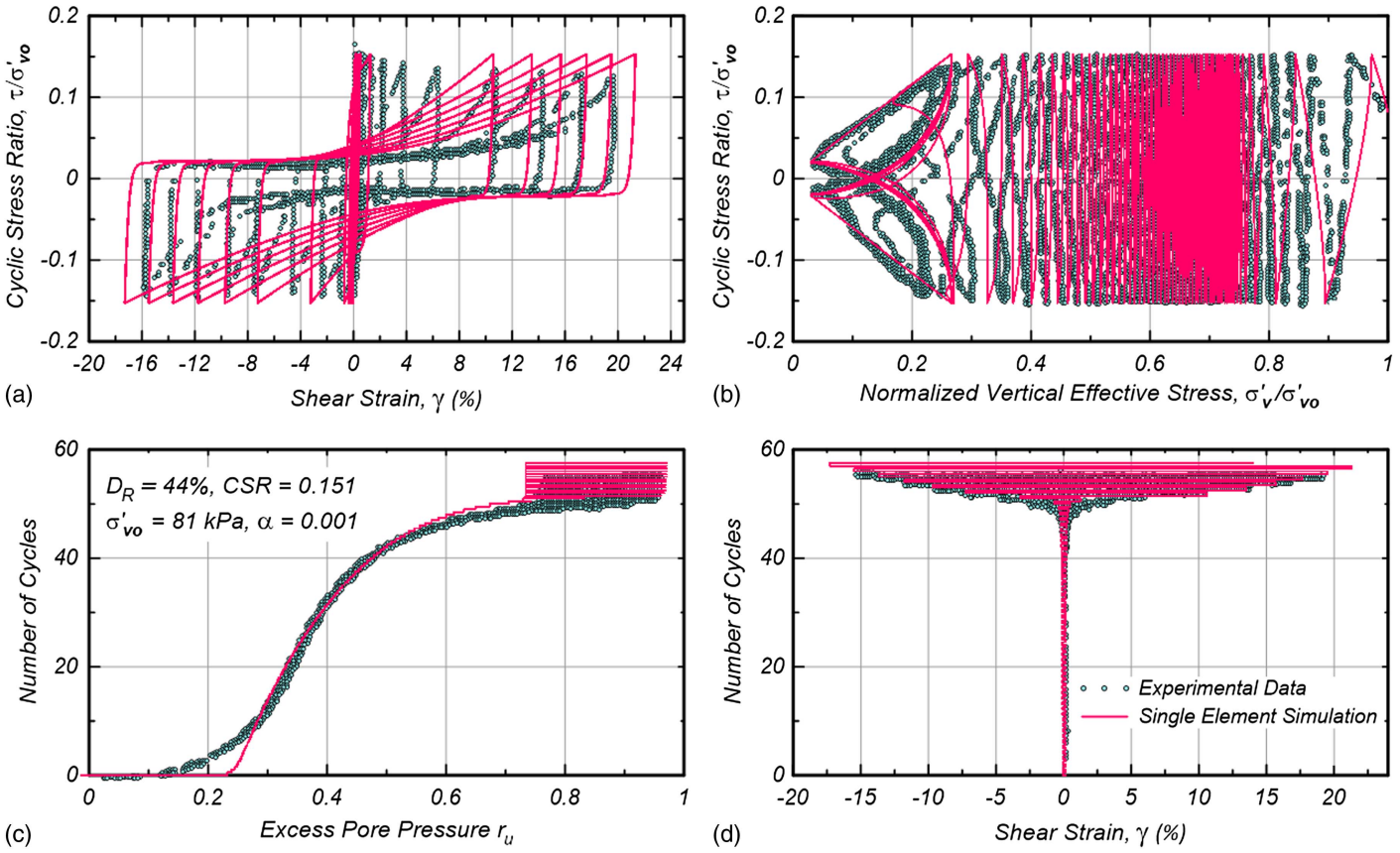

Fig. 15. Comparison between single element simulation and experimental data from Wu (2002) under undrained DSS loading conditions for Monterey sand with $D_R = 44\%$: (a) stress-strain loops; (b) effective stress paths; (c) excess pore pressure evolution with number of cycles; and (d) stress-strain versus number of loading cycles.

the apparent relative density, D_{Ro}, assigned to the model, which was given the value of 44%.

Comparison of Calibrated Numerical Model Prediction with Experimental Results

The tube uplift observed in the centrifuge experiment is primarily related to the movement of the surrounding soil towards and underneath the tube, resulting in a sideways and upwards push of the lighter tunnel by the heavier and softened liquefiable soil (Travasarou et al. 2011; Chou et al. 2011). In particular, Travasarou et al. (2011) state that "the buried structure is effectively driven by the displacement of the weakened—by the generated pore pressure—soil in response to the alternate cycles of strong ground motion in a ratcheting manner," and relate the primary source of uplift to shearing of the liquefiable backfill soils. Fig. 16 illustrates and compares the deformation patterns observed in the experiment and the numerical analysis. In both cases, it is indicated that soil displacement occurs toward and beneath the tunnel, while the maximum shearing occurs within the foundation course layer consisting of Monterey sand with $D_R = 40\%$.

Simple shear conditions are predominant where shear zones are developed. This is the case for the foundation course layer as indicated in Fig. 17, which plots time histories of angle α between the direction of maximum principal stress and the vertical at three different locations [locations shown in Fig. 16(b)]. Angle α represents the level of principal stress rotation, and thus the loading direction, and it is defined in Yoshimine et al. (1998) and Nakata et al. (1998)

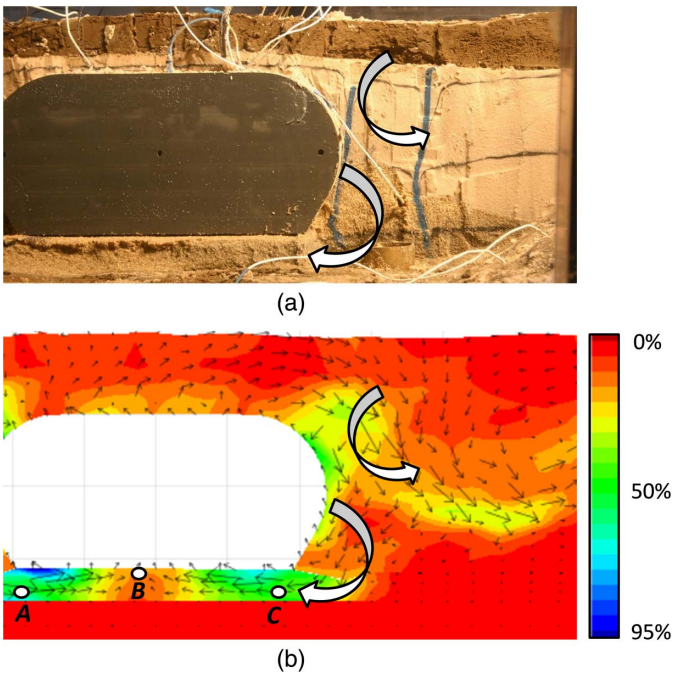

Fig. 16. Displacement of sand toward and beneath the tunnel from (a) experimental observation; and (b) numerical analysis. The deformation pattern is illustrated through vertical sand columns for the centrifuge test and displacement vectors and shear strain contours for the numerical analysis.

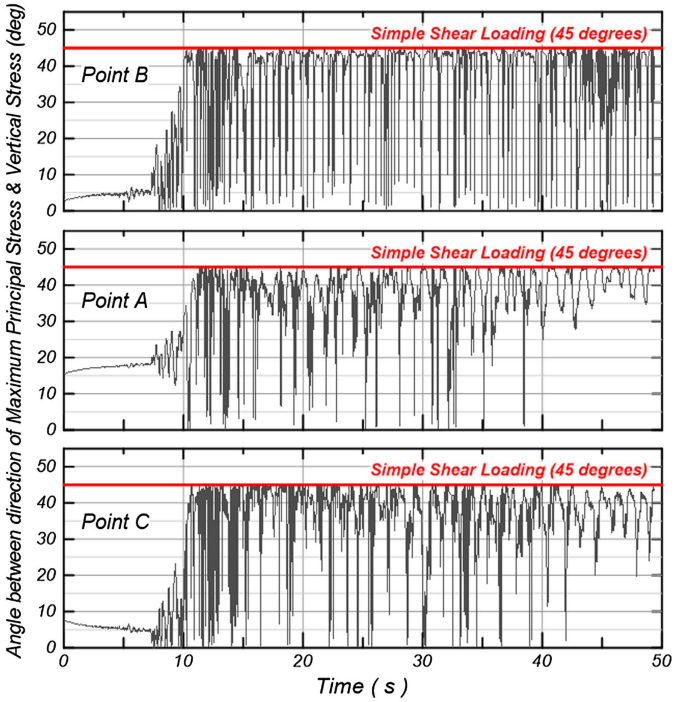

Fig. 17. Time histories of angle α between the direction of the maximum principal stress and the vertical obtained from numerical analysis at three locations within the foundation course of Monterey sand with $D_R = 40\%$, shown in Fig. 16(b).

$$\alpha = \frac{1}{2}\tan^{-1}\left(\frac{\sigma_{12}}{\sigma_{11} - \sigma_{22}}\right) \tag{6}$$

where σ_{12} = shear stress; σ_{11} = vertical effective stress; and σ_{22} = in-plane horizontal effective stress. For triaxial compression, $\alpha = 0°$, whereas in triaxial extension, $\alpha = 90°$. The angle α under simple shear loading and an isotropic initial consolidation state ($K_0 = 1$) is equal to 45°. Fig. 17 demonstrates that during most of the earthquake, angle α is close to 45°, indicating simple shear loading conditions. Transiently, when the shear stress is near zero during reversals, the angle α becomes ~0°. The amount of soil volume moving beneath the tunnel in combination with the shearing of the foundation course layer, both affected by the ratcheting deformation mechanism of the tunnel, are critical parameters to the level of tunnel-uplift developed.

The comparison between numerical and experimental results is conducted in terms of tunnel uplift at the location of the displacement transducer DVT1 and pore pressure within the foundation course at location P5 (Fig. 11). The numerical and experimental time histories of tunnel uplift and pore pressure are plotted together with the acceleration time history of the input motion in Fig. 18, and the simulations compare well with the experimental data. Liquefaction occurs at ~12 s indicated by the abrupt increase of pore pressure. The upward movement of the tunnel begins at that moment, and it is developed under the postliquefaction regime. As such, the accuracy of the numerical prediction is affected by the appropriate calibration of the constitutive model not only for liquefaction triggering but also for postliquefaction shear strain accumulation. In addition, comparison between experimental and numerical responses in terms of the trajectory of the vertical movement, measured at the center of the tunnel relative to the container base as a function of the tunnel horizontal displacement of the tunnel relative to the clay trench (Fig. 19), reveals that the ratcheting mechanism was sufficiently captured by the numerical analysis.

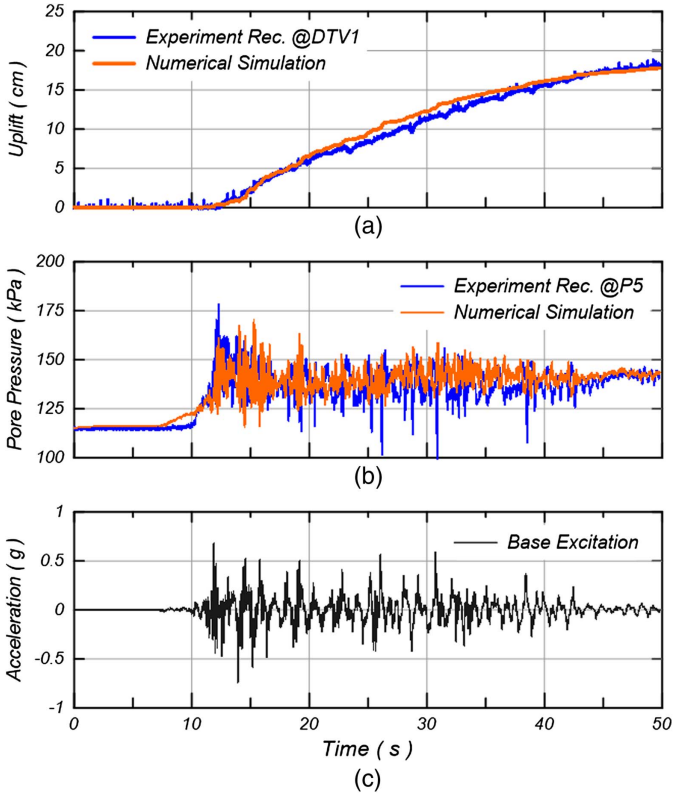

Fig. 18. Comparison between numerical and centrifuge results for BART Transbay tube (Fig. 12) in terms of time histories of (a) tunnel uplift (DVT1); (b) pore pressure (P5); and (c) acceleration time history applied at the base of both centrifuge and numerical models in prototype scale.

Liquefaction-Induced Lateral Spreading Demands on Sheet Pile Quay Wall

A series of dynamic centrifuge experiments were conducted in Shimizu's Institute of Technology, Japan (Sato et al. 2001), to evaluate the seismic response of quay walls and adjacent structures subject to large liquefaction-induced lateral spreading. These experiments were previously used for validation by Tasiopoulou et al. (2013, 2019). The centrifuge models were placed in a laminar box and subjected to a 30 g acceleration field. Silicon oil, with a viscosity 30 times higher than that of water, was used for saturation of the soil deposit to achieve a single scale for both dynamic and diffusion time. Centrifuge Model 1 from Sato et al. (2001), depicted in Fig. 20, contained a floating sheet pile quay wall behind a waterfront area. The backfill consists of four layers, including a liquefiable layer of relatively loose sand being 4.2 m thick that underlies a surficial equally loose but unsaturated layer and overlies two layers of dense non-liquefiable sand. The base of the model was excited by a 2 Hz sinusoidal motion with 4–5 cycles of 0.2 g maximum acceleration followed by 8–9 cycles of higher amplitude with a maximum value of 0.65 g in the prototype scale [Fig. 21(c)].

Fig. 20(b) shows the numerical grid in FLAC 8 (Itasca 2016) of the centrifuge experiment described in the preceding prototype scale. The selected element size was 0.5 m. The boundaries of the model simulated a stiff laminar box behavior. Due to lack of

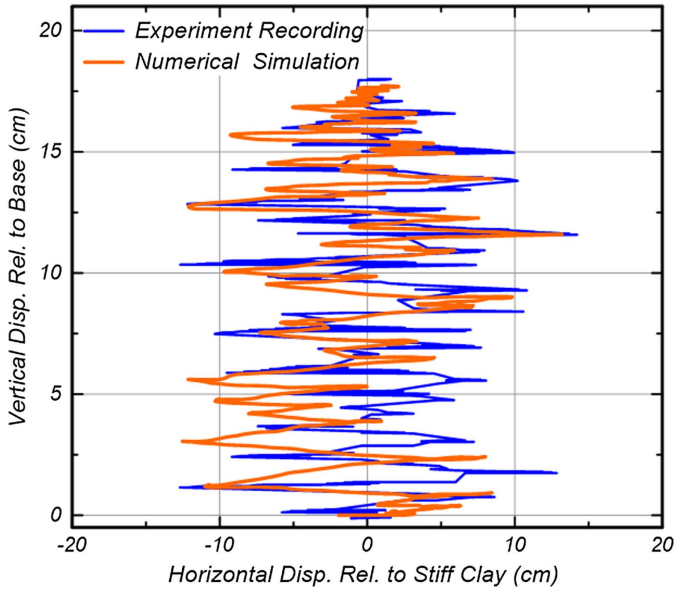

Fig. 19. Comparison between experimental and numerical response in terms of the trajectory of the vertical movement measured at the center of tunnel relative to the container base as a function of the tunnel horizontal displacement relative to the clay trench, indicating a ratcheting mechanism.

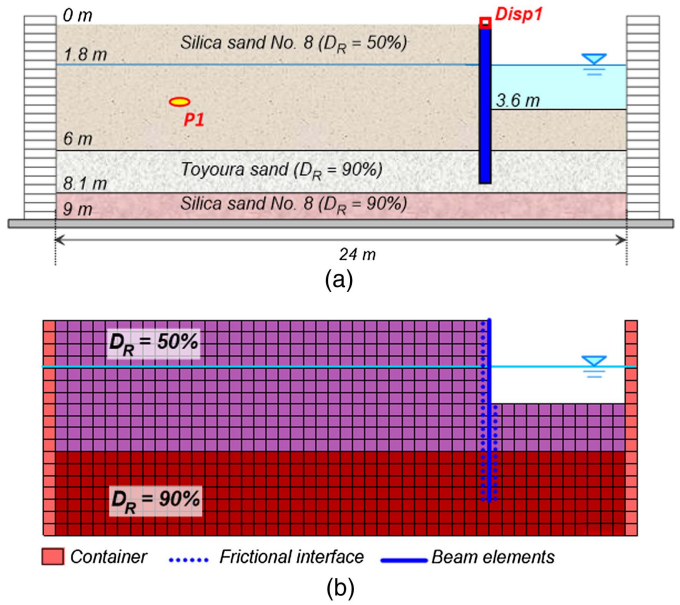

Fig. 20. (a) Centrifuge model; and (b) numerical model of sheet pile quay wall retaining liquefiable backfill in prototype scale.

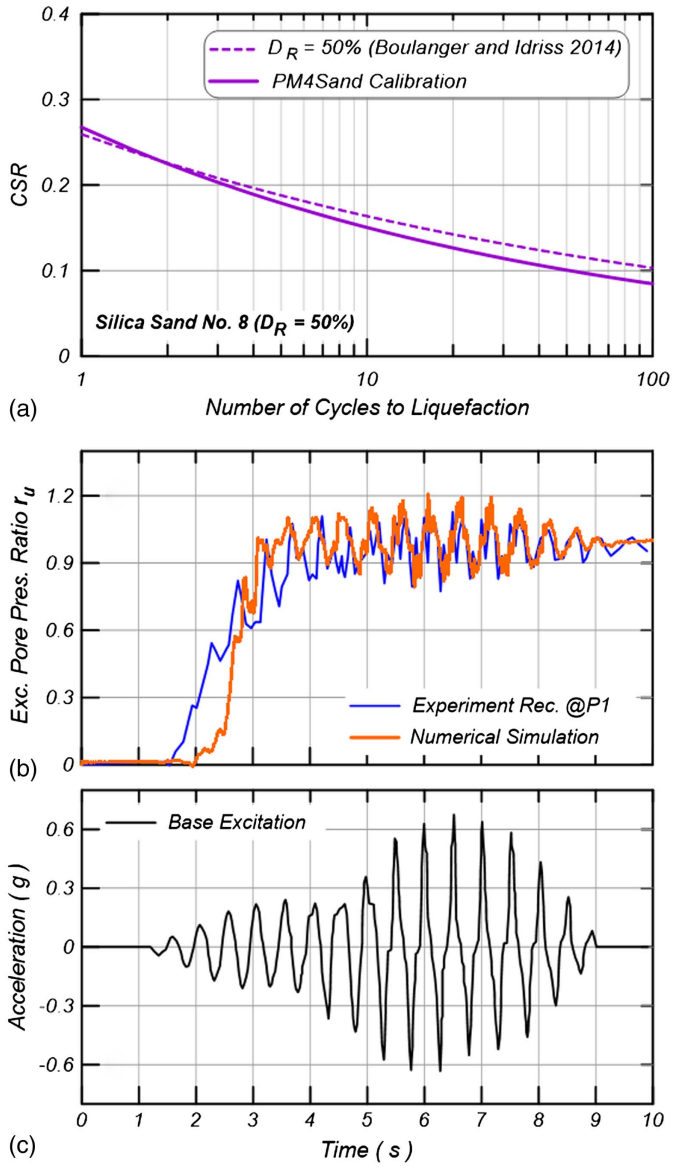

Fig. 21. (a) Liquefaction resistance curve for liquefiable backfill ($D_R = 50\%$) obtained from PM4Sand single element simulations against empirical curves; (b) comparison between numerical and centrifuge results for sheet pile quay wall retaining liquefiable backfill (Fig. 20) in terms of time histories of excess pore pressure ratio, r_u (P1); and (c) acceleration time history applied at the base of both centrifuge and numerical models in prototype scale.

detailed information on the laminar container used in the centrifuge, solid elastic elements with a Young's modulus of 100 MPa were used. The elastic solid elements at the boundaries of the model were constrained to move together in the horizontal direction. The floating sheet-pile quay wall was simulated using linear beam elements. The behavior of the beam elements was described with four parameters: mass density, ρ; Young's modulus, E; sheet cross-section area, A; and moment of inertia, I. The properties used for the structural elements in prototype scale are provided by Sato et al. (2001). Coulomb frictional interfaces with an interface friction angle of 30° were used for the contact between the quay wall and the surrounding soil. The permeability assigned to the soil was equal to 0.003 cm/s. All sand layers were modeled with PM4sand.

Constitutive Model Calibration of Coarse-Grain Materials without Soil-Specific Lab Data

Calibration of PM4sand for this numerical simulation was based on the median (i.e., using a C_0 value of 2.6) empirical liquefaction resistance curves by Boulanger and Idriss (2014) due to lack of experimental data on the liquefiable layer of Silica sand No. 8. The median curves were selected as a *best-estimate* for modeling a test, rather than the 16th percentile (C_0 value of 2.8) commonly used in engineering design. The median empirical liquefaction

J. Geotech. Geoenviron. Eng., 2020, 146(1): 04019120

Table 4. Model parameters for the numerical simulation of the sheet pile quay wall centrifuge test

Target behavior	PM4Sand parameters	$D_R = 50\%$ Best estimate	$D_R = 50\%$ Higher strain estimate	$D_R = 50\%$ Lower strain estimate	$D_R = 90\%$
Liquefaction triggering	D_R	50%	50%	50%	90%
	n^b	0.1	0.1	0.1	Default
	G_0	Default	Default	Default	Default
	h_{p0}	0.4	0.4	0.4	0.08
Postliquefaction shear strain	C_ε	5	100	0.01	Default
	z_{max}	Default	50	0.1	Default

resistance curves selected correspond to values of relative density equal to 50% and 90% for the liquefiable and non-liquefiable layers, respectively. In calibrating PM4Sand for postliquefaction shear strain accumulation, three scenarios were targeted, all using the same liquefaction resistance curve: (1) a best estimate scenario in which the median compliance rate, $\Delta\gamma_{postliq}\,per\,cycle/\tau_{cyc}$, was targeted using $B = 28$ in Eq. (3) (see also Fig. 10); (2) a higher strain scenario targeting above the upper bound curve corresponding to the 95th percentile (Fig. 10); and (3) a lower strain scenario targeting below the lower bound corresponding to the fifth percentile (Fig. 10). Single element simulations using PM4Sand were performed to develop a set of model parameters for the liquefiable ($D_R = 50\%$) and non-liquefiable ($D_R = 90\%$) layers, with the results of the calibration in terms of primary and secondary PM4Sand parameters shown in Table 4. Please note that for this case, only two parameters were adjusted to capture variations in the target compliance rate. However, because the responses of the system are inter-related, this approach may not be universally applicable.

Comparison of Calibrated Numerical Model Prediction with Experimental Results

Liquefaction-induced lateral spreading of the backfill leads to outward displacement and rotation of the sheet pile quay wall. The liquefaction resistance curve for the liquefiable backfill consisting of Silica sand No. 8 with $D_R = 50\%$ obtained using the sets of parameters on Table 4 is compared to the median empirical curve of Boulanger and Idriss (2014) in Fig. 21(a). Fig. 21(b) compares numerically and experimentally obtained excess pore pressure ratio time histories in the free field (location P1 in Fig. 20). The figure indicates an agreement in the experimental and numerically predicted initiation of liquefaction at ~3 s ($r_u > 0.8$) after 3 loading cycles. The input acceleration time history applied at the base of the model is illustrated in Fig. 21(c). This agreement in liquefaction initiation affirms the applicability of the empirical Boulanger and Idriss (2014) liquefaction resistance curve in the absence of experimental data.

The ranges of the compliance rate, $\Delta\gamma_{postliq}\,per\,cycle/\tau_{cyc}$, obtained from single element simulations for the three calibration scenarios of best, higher, and lower strain estimates, described in the previous subsection, are plotted in Fig. 22(a) together with the generic semiempirical postliquefaction shear strain curves corresponding to the median fit and the 90% confidence interval bounded by the 5th and 95th percentile relationships. Time histories of lateral displacement of the sheet-pile quay wall at the top for the three calibration scenarios used in the numerical simulations are compared to the centrifuge results in Fig. 22(b). Liquefaction triggering occurs after the first three cycles of loading for all three numerical estimates because they are calibrated to a common liquefaction resistance curve [Fig. 21(a)]. As such, during the first three

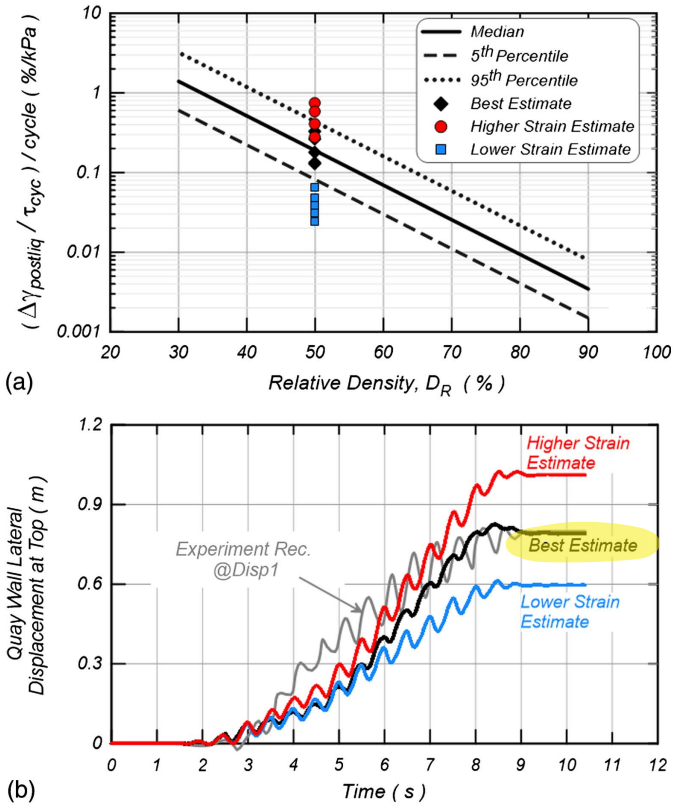

Fig. 22. (a) Postliquefaction compliance rate for liquefiable ($D_R = 50\%$) layer obtained from PM4Sand single element simulations against semiempirical curves for three strain level estimates; and (b) comparison between numerical and centrifuge results for sheet pile quay wall retaining liquefiable backfill (Fig. 20) in terms of time histories of quay wall horizontal displacement at the top (Disp1).

loading cycles, until 3 s approximately, the displacement time histories agree for the three estimation scenarios. Accumulation of outward displacement of the quay wall occurs under the postliquefaction regime until a residual value is reached at the end of shaking. Fig. 23(a) illustrates a shear zone developed within the liquefied layer close to the interface with the dense sand layer. Shear stress-strain loops and shear strain time histories, for the best-estimate scenario depicted in Fig. 23(b) at three different locations within the shear zone, indicate a gradual decrease of the shear stresses propagated upwards (with increases in excess pore water pressure) accompanied with an accumulation of shear strains in the seaward direction. The magnitude of the shear strains is inversely proportional to the distance of each location from the quay wall; a pattern also observed in the centrifuge test.

The best-estimate analysis produces the most successful comparison with the centrifuge experiment, in terms of the residual quay wall displacement equal to 0.8 m, even though the simulated displacement time history does not perfectly fit the experiment. This discrepancy may have been limited by fine-tuning other aspects of the analysis, such as the modeling of the laminar box (thus, the inertial response of the sidewalls) along with the calibration of the dense sand layer, which provides the main source of resistance against the outward movement of the quay-wall depending greatly on the suction developed. Unfortunately, there was no instrumentation to evaluate the experimental behavior of this dense sand unit.

Cases with limited site-specific data requiring basic assumptions and judgment are commonly encountered in engineering practice.

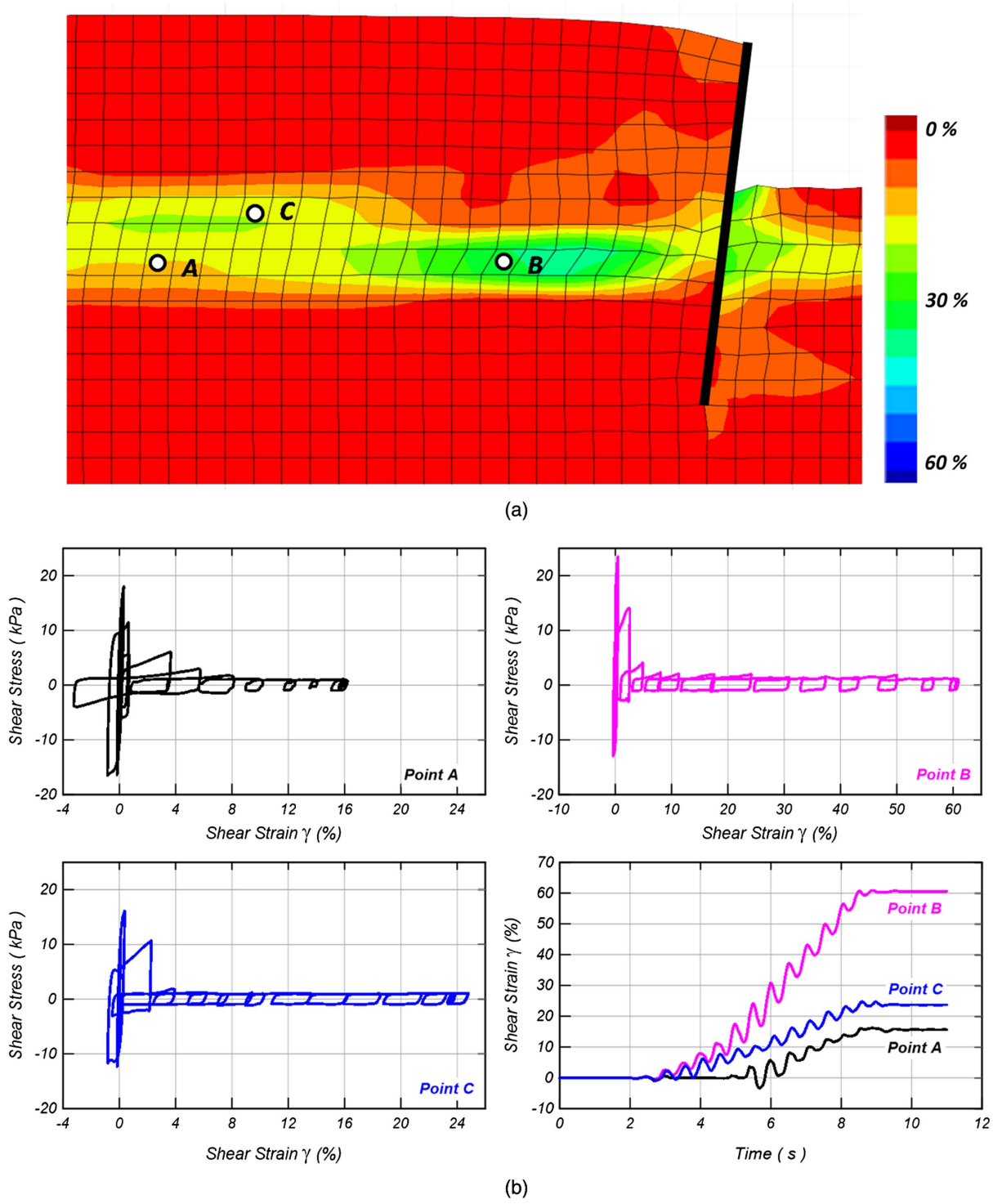

Fig. 23. (a) Shear strain contours at the end of shaking; and (b) shear stress-strain loops along with shear strain time histories at three different locations within the liquefiable backfill ($D_R = 50\%$).

In such cases, it is usual to refer to empirical relationships found in the literature and perform parametric analyses. This simulation attempted to reproduce a similar case using empirical frameworks related to liquefaction. In that context, the best-estimate analysis is considered successful in predicting the residual quay wall displacement. The higher and lower strain scenarios lead to residual quay wall displacements of 1 and 0.6 m, respectively, either overpredicting or underpredicting the residual centrifuge results by approximately 25%. These parametric analyses highlight the significance of calibrating not only for liquefaction triggering but also for postliquefaction shear strain accumulation, particularly for cases in which liquefaction-induced deformations are the predominant mode of failure. In retrospect, it is worth noting that for this example, even in the absence of soil-specific experimental data, the range of compliance rates suggested by the generic semiempirical postliquefaction shear strain curves, combined with empirical liquefaction resistance curves, provided a reasonable prediction of the system deformation.

Discussion and Conclusions

A plethora of empirical correlations are available to estimate liquefaction triggering of sand-like materials, which is typically defined to be concurrent with shear strains of about 3%. However, very little guidance is available for the estimation of post-triggering shear deformations. The latter may be equally important for the prediction of liquefaction-induced deformations, especially if liquefaction is triggered early in the earthquake.

A framework for the estimation of deformations in the postliquefaction regime has been developed based on an extensive database of available cyclic simple and torsional shear tests on medium to dense clean sands samples without static shear bias. Based on fundamental experimental observations, a compliance rate has been defined as the postliquefaction shear strain rate per cycle over the shear stress amplitude. Semiempirical relationships of the compliance rate as a function of the relative density have been developed to provide guidance for estimating postliquefaction shear strains for five types of sand as well as a more generic fit (with associated uncertainties) for the whole body of experimental data collected. The plots and equations developed thereafter provided guidance for estimating postliquefaction shear strains as a function of soil relative density, cyclic loading level, and number of loading cycles expected postliquefaction. Because these are parameters normally considered in liquefaction triggering evaluations, the approach can readily be used in practical applications.

Realistic and reliable estimates of liquefaction-induced deformations normally require the use of nonlinear dynamic analyses. The proposed framework was used for the calibration of a comprehensive liquefaction constitutive model (PM4Sand) implemented in a widely used finite difference code (FLAC 8). A calibration methodology was developed giving emphasis to both liquefaction triggering and postliquefaction accumulation of deformations. Two well-documented centrifuge tests focusing on liquefaction-induced demands on engineering structures were simulated to validate the ability of the proposed calibration methodology to predict liquefaction-induced deformations. In one simulation available, soil-specific laboratory data were used for model calibration; while in the other simulation, the model parameters were calibrated based on generic empirical liquefaction resistance curves and semiempirical postliquefaction shear strain curves presented in this paper. It was shown that numerical analyses using calibrated numerical models capable of capturing both liquefaction triggering and postliquefaction deformations (using the framework proposed in this paper) led to successful reproduction of measured system responses.

It is common practice in NDAs to calibrate advanced constitutive models against available lab data (typically cyclic direct simple shear or triaxial tests) and/or the cumulative body of data (as captured by empirical and semiempirical relationships) and to then use these calibrated models in simulations where more complicated loading paths develop. It would be extremely challenging to predict the loading paths that would develop in a real problem and even more so to reproduce them in the lab in order to calibrate a constitutive model. That is why validation of system level behaviors (and not only element level calibration) is a critical part of NDAs using advanced constitutive models and also why well-documented centrifuge experiments containing structures and complex geometries/stratigraphy were chosen for testing the proposed framework. Such a framework provides a basis to calibrate models used in NDAs of shear-induced deformation problems in liquefiable sand.

The proposed framework was built on an extensive database of cyclic simple shear and torsional tests on clean siliceous sands without static shear bias. However, the robustness of the findings and the quantification of uncertainties could be enhanced by supplementing the underlying database. Further research is needed to evaluate the influence of factors such as static shear stress and fines content on the trends identified in this study. Lastly, fundamental studies to better define the phenomena underlying the empirical trends would build confidence in the findings. However, this study provides a previously missing basis for the quantification of postliquefaction deformations and the calibration of comprehensive liquefaction models that are a key component in numerical analyses for the performance-based design of engineering structures.

Data Availability Statement

Some data used during the study are available from the corresponding author by request.

Acknowledgments

The research related to this study was partially funded by FUGRO, whose support is gratefully acknowledged. The authors are also grateful to Dr. Kumar S. Sriskandakumar for sharing his data from experiments performed at the University of British Columbia under the supervision of Professor Dharma Wijewickreme. The authors' work benefited greatly from discussions with Dr. Vasileios Drosos of GR8 GEO and Professor Ross W. Boulanger of the University of California, Davis.

References

Andrus, R. D., and K. H. Stokoe, II. 1997. "Liquefaction resistance based on shear wave velocity." In *Proc., NCEER Workshop on Evaluation of Liquefaction Resistance of Soils, National Center for Earthquake Engineering Research*, 89–128. Buffalo, NY: State Univ. of New York.

Arulmoli, K., K. K. Muraleetharan, M. M. Hossain, and L. S. Fruth. 1992. *VELACS: Verification of liquefaction analysis by centrifuge studies, laboratory testing program*. Soil Data Rep., Project No. 90–0562. Irvine, CA: Earth Technology Corporation.

Bartlett, S. F., and T. L. Youd. 1995. "Empirical prediction of liquefaction-induced lateral spread." *J. Geotech. Eng.* 121 (4): 316–329. https://doi.org/10.1061/(ASCE)0733-9410(1995)121:4(316).

Beaty, M., and P. M. Byrne. 1998. "An effective stress model for predicting liquefaction behavior of sand." In *Proc., Specialty Conf., Geotechnical Earthquake Engineering and Soil Dynamics*, 766–777. Reston, VA: ASCE.

Been, K., and M. G. Jefferies. 1985. "A state parameter for sands." *Géotechnique.* 35 (2): 99–112. https://doi.org/10.1680/geot.1985.35.2.99.

Bolton, M. D. 1986. "The strength and dilatancy of sands." *Géotechnique.* 36 (1): 65–78. https://doi.org/10.1680/geot.1986.36.1.65.

Boulanger, R. W., and I. M. Idriss. 2014. *CPT and SPT based liquefaction triggering procedures*. Rep. No. UCD/CGM-14/01. Davis, CA: Univ. of California, Davis.

Boulanger, R. W., I. M. Idriss, and L. H. Mejia. 1995. *Investigation and evaluation of liquefaction related ground displacements at Moss Landing during the 1989 Loma Prieta earthquake*. Rep. No. UCD/CGM-95/02. Davis, CA: Univ. of California, Davis.

Boulanger, R. W., and K. Ziotopoulou. 2017. *A sand plasticity model for earthquake engineering applications: Version 3.1*. Rep. No. UCD/CGM-17-01. Davis, CA: Univ. of California, Davis.

Boulanger, R. W., and K. Ziotopoulou. 2018. "On NDA practices for evaluating liquefaction effects." In *Proc., Geotechnical Earthquake Engineering and Soil Dynamics V.* Reston, VA: ASCE.

Casagrande, A. 1976. *Liquefaction and cyclic deformation of sands: A critical review. No. 88 of Harvard soil mechanics series*. Cambridge, MA: Harvard Univ.

Castro, G. 1975. "Liquefaction and cyclic mobility of saturated sands." *J. Geotech. Eng. Div.* 101 (GT6): 551–569.

Castro, G., and S. J. Poulos. 1977. "Factors affecting liquefaction and cyclic mobility." *J. Geotech. Eng. Div.* 103 (GT6): 501–516.

CESMD (Center for Engineering Strong Motion Data). 1999. "Strong motion virtual data center." Accessed February 10, 2015. https://strongmotioncenter.org/vdc/scripts/event.plx?evt=629.

Chiaro, G., J. Koseki, and T. Sato. 2012. "Effects of initial static shear on liquefaction and large deformation properties of loose saturated Toyoura sand in undrained cyclic torsional shear tests." *Soils Found.* 52 (3): 498–510. https://doi.org/10.1016/j.sandf.2012.05.008.

Chiaro, H., T. Kiyota, L. I. N. De Silva, T. Sato, and J. Koseki. 2009. "Extremely large post-liquefaction deformations of saturated sand under cyclic torsional shear loading." In *Proc., 13th Int. Conf. on Soil Mechanics and Geotechnical Engineering, Earthquake Geotechnical Engineering Satellite Conf.* Seattle: Allen Institute for Artificial Intelligence.

Chou, J. C., B. L. Kutter, and T. Travasarou. 2008. *Centrifuge testing of the seismic performance of a cut-and-cover tunnel in liquefiable soil: Centrifuge data report for test series JCC01*. Rep. No. UCD/CGMDR-07/08-JCC01. Davis, CA: Univ. of California, Davis.

Chou, J. C., B. L. Kutter, T. Travasarou, and J. M. Chacko. 2011. "Centrifuge modeling of seismically induced uplift for the BART Transbay tube." *J. Geotech. Geoenviron. Eng.* 137 (8): 754–765. https://doi.org/10.1061/(ASCE)GT.1943-5606.0000489.

Cubrinovski, M., J. D. Bray, M. Taylor, S. Giorgini, B. Bradley, L. Wotherspoon, and J. Zupan. 2011. "Soil liquefaction effects in the central business district during the February 2011 Christchurch earthquake." *Seismol. Res. Lett.* 82 (6): 893–904. https://doi.org/10.1785/gssrl.82.6.893.

Dafalias, Y. F., and M. T. Manzari. 2004. "Simple plasticity sand model accounting for fabric change effects." *J. Eng. Mech.* 130 (6): 622–634. https://doi.org/10.1061/(ASCE)0733-9399(2004)130:6(622).

Darendeli, M. B. 2001. "Development of a new family of normalized moduli reduction and material damping curves." Ph.D. dissertation, Dept. of Civil, Architectural and Environmental Engineering, Univ. of Texas at Austin.

De Alba, P., H. B. Seed, and C. K. Chan. 1976. "Sand liquefaction in large-scale simple shear tests." *J. Soil Mech. Found. Div.* 102 (GT9): 909–927.

De Silva, L. I. N., J. Koseki, G. Chiaro, and T. Sato. 2015. "A stress-strain description of saturated sand under undrained cyclic torsional shear loading." *Soils Found.* 55 (3): 559–574. https://doi.org/10.1016/j.sandf.2015.04.008.

Doygun, O. 2009. "Monotonic and cyclic undrained loading behavior of intermediate soils." M.Sc. dissertation, Dept. of Civil and Environmental Engineering, Technische Univ. Darmstadt.

Elgamal, A., R. Dobry, E. Parra, and Z. Yang. 1998. "Soil dilation and shear deformations during liquefaction." In *Proc: 4th Int. Conf. on Case Histories in Geotechnical Engineering*. Rolla, MO: Univ. of Missouri.

Elgamal, A., Z. Yang, E. Parra, and A. Ragheb. 2003. "Modeling of cyclic mobility in saturated cohesionless soils." *Int. J. Plast.* 19 (6): 883–905. https://doi.org/10.1016/S0749-6419(02)00010-4.

Giannakou, A., T. Travasarou, J. Ugalde, J. M. Chacko, and P. M. Byrne. 2011. "Calibration methodology for liquefaction problems considering level and sloping ground conditions." In *Proc., 5th Int. Conf. on Earthquake Geotechnical Engineering*. Santiago, Chile: Chilean Geotechnical Society.

Hamada, M., and T. D. O'Rourke. 1992. *Case studies of liquefaction and lifeline performance during past earthquakes. Volume 1 Japanese case studies*. Technical Rep. No. NCEER-92-0001. Buffalo, NY: National Center for Engineering Research.

Hamada, M., I. Towhata, S. Yasuda, and R. Isoyama. 1987. "Study on permanent ground displacement induced by seismic liquefaction." *Comput. Geotech.* 4 (4): 197–220. https://doi.org/10.1016/0266-352X(87)90001-2.

Hatanaka, M., A. Uchida, and J. Ohara. 1997. "Liquefaction characteristics of a gravelly fill liquefied during the 1995 Hyogo-Ken Nanbu earthquake." *Soils Found.* 37 (3): 107–115. https://doi.org/10.3208/sandf.37.3_107.

Idriss, I. M. 1990. "Response of soft soil sites during earthquakes." In Vol. 2 of *Proc., H. Bolton Seed Memorial Symp.*, 273–289. Vancouver, Canada: BiTech Publishers.

Idriss, I. M., and R. W. Boulanger. 2008. *Soil liquefaction during earthquakes*. Monograph MNO-12. Oakland, CA: Earthquake Engineering Research Institute.

Ishihara, K. 1985. "Stability of natural deposits during earthquakes." In *Proc., 11th Int. Conf. on Soil Mechanics and Foundation Engineering*, 321–376. Rotterdam, Netherlands: A.A. Balkema.

Itasca. 2016. *FLAC—Fast Lagrangian Analysis of Continua, version 8.0*. Minneapolis: Itasca Consulting Group.

Kammerer, A. M., J. Wu, J. M. Pestana, M. Riemer, and R. B. Seed. 2000. *Cyclic simple shear testing of Nevada sand for PEER center project 2051999*. Geotechnical Engineering Rep. No. UCBGT-2000-01. Berkeley, CA: Univ. of California, Berkeley.

Khosravifar, A., A. Elgamal, J. Lu, and J. Li. 2018. "A 3D model for earthquake-induced liquefaction triggering and post-liquefaction response." *Soil Dyn. Earthquake Eng.* 110 (Jul): 43–52. https://doi.org/10.1016/j.soildyn.2018.04.008.

Kiyota, T., J. Koseki, and T. Sato. 2010. "Comparison of liquefaction-induced ground deformation between results from undrained cyclic torsional shear tests and observations from previous model tests and case studies." *Soils Found.* 50 (3): 421–429. https://doi.org/10.3208/sandf.50.421.

Kiyota, T., T. Sato, J. Koseki, and M. Abadimarand. 2008. "Behavior of liquefied sands under extremely large strain levels in cyclic torsional shear tests." *Soils Found.* 48 (5): 727–739. https://doi.org/10.3208/sandf.48.727.

Kramer, S. L., and P. Arduino. 1999. "Constitutive modeling of cyclic mobility and implications for site response." In *Proc. 2nd Int. Conf. on Earthquake Geotechnical Engineering*, edited by Pedro S. Seco e Pinto, 1029–1034. Rotterdam, Netherlands: A.A. Balkema.

Kutter, B. L., Y. Chen, and C. K. Shen. 1994. *Triaxial and torsional shear test results for sand*. Contact Rep. No. CR 94.003-SHR. Port Hueneme, CA: Naval Facilities Engineering Service Center.

Lee, F. H., and A. N. Schofield. 1988. "Centrifuge modelling of sand embankments and islands in earthquakes." *Géotechnique.* 38 (1): 45–58. https://doi.org/10.1680/geot.1988.38.1.45.

Lee, W. H. K., and T. C. Shin. 2001. "Strong-motion instrumentation and data." Supplement, *Earthquake Spectra* 17 (S1): 5–18. https://doi.org/10.1193/1.1586190.

Nakata, Y., M. Hyodo, H. Murata, and N. Yasufuku. 1998. "Flow deformation of sands subjected to principal stress rotation." *Soils Found.* 38 (2): 115–128. https://doi.org/10.3208/sandf.38.2_115.

Parra Bastidas, A. M. 2016. "Ottawa F-65 sand characterization." Ph.D. dissertation, Dept. of Civil and Environmental Engineering, Univ. of California, Davis.

Rauch, A. F., and J. R. Martin, II. 2000. "EPOLLS model for predicting average displacements on lateral spreads." *J. Geotech. Geoenviron. Eng.* 126 (4): 360–371. https://doi.org/10.1061/(ASCE)1090-0241(2000)126:4(360).

Sato, M., T. Tazoh, and M. Ogasawara. 2001. "Reproduction of lateral ground displacement and lateral flow—Earth pressure acting on pile foundations using centrifuge modeling." In *Proc., 4th Int. Conf. on Recent Advances in Geotechnical Earthquake Engineering and Soil Dynamics Symp.*, edited by S. Prakash. Rolla, MO: Univ. of Missouri–Rolla.

Seed, H. B. 1979. "Soil liquefaction and cyclic mobility evaluation for level ground during earthquakes." *J. Geotech. Eng. Div.* 105 (GT2): 201–255.

Seed, H. B., and I. M. Idriss. 1982. *Ground motions and soil liquefaction during earthquakes*. Oakland, CA: Earthquake Engineering Research Institute.

Seed, H. B., and K. L. Lee. 1966. "Liquefaction of saturated sands during cyclic loading." *J. Soil Mech. Found. Eng. Div.* 92 (SM6): 105–134.

Seed, H. B., K. L. Lee, I. M. Idriss, and F. Makdisi. 1975. "The slides in the San Fernando dams during the earthquake of February 9, 1971." *J. Geotech. Eng. Div.* 101 (GT7): 651–688.

Sento, N., and A. Shimazaki. 2013. "Shear strain development characteristics of saturated sand slope considering aftershock effect."

[In Japanese.] In *Proc., 2013 Annual Meeting of Japanese Society of Civil Engineers*, 651–652. Tokyo: Japanese Society of Civil Engineers.
Shamoto, Y., J. M. Zhang, and S. Goto. 1997. "Mechanism of large post-liquefaction deformation in saturated sand." *Soils Found.* 37 (2): 71–80. https://doi.org/10.3208/sandf.37.2_71.
Shamoto, Y., J. M. Zhang, and K. Tokimatsu. 1998a. "New charts for predicting large residual post-liquefaction ground deformation." *Soil Dyn. Earthquake Eng.* 17 (7): 427–438. https://doi.org/10.1016/S0267-7261(98)00011-6.
Shamoto, Y., J. M. Zhang, and K. Tokimatsu. 1998b. "Methods for evaluating large residual post-liquefaction ground settlement and horizontal displacement." Supplement, *Soils Found.* 38 (S2): 69–83. https://doi.org/10.3208/sandf.38.Special_69.
Sivathayalan, S., and D. Ha. 2011. "Effect of static shear stress on the cyclic resistance of sands in simple shear loading." *Can. Geotech. J.* 48 (10): 1471–1484. https://doi.org/10.1139/t11-056.
Sriskandakumar, S. 2004. "Cyclic loading response of Fraser River sand for validation of numerical models simulating centrifuge tests." M.Sc. thesis, Dept. of Civil Engineering, Univ. of British Columbia.
Tasiopoulou, P., and N. Gerolymos. 2016. "Constitutive modeling for sand: Formulation of a new plasticity approach." *Soil Dyn. Earthquake Eng.* 82 (Mar): 205–221. https://doi.org/10.1016/j.soildyn.2015.12.014.
Tasiopoulou, P., N. Gerolymos, T. Tazoh, and G. Gazetas. 2013. "Pile-group response to large soil displacements and liquefaction: Centrifuge experiments versus a physically simplified analysis." *J. Geotech. Geoenviron. Eng.* 139 (2): 223–233. https://doi.org/10.1061/(ASCE)GT.1943-5606.0000759.
Tasiopoulou, P., A. Giannakou, V. Drosos, P. Georgarakos, J. Chacko, S. de Wit, and N. Zuideveld-Venema. 2019. "Numerical evaluation of dynamic levee performance due to induced seismicity." *Bull. Earthquake Eng.* 17 (8): 4559–4574. https://doi.org/10.1007/s10518-018-0426-5.
Tatsuoka, F., and K. Ishihara. 1973. "Stress path and dilatancy performance of sand." In Vol. 1 of *Proc., 8th Int. Conf. on Soil Mechanics and Foundation Engineering*, 419–424. London: International Society of Soil Mechanics and Foundation Engineering.
Tatsuoka, F., K. Ochi, S. Fujii, and M. Okamoto. 1986. "Cyclic undrained triaxial and torsional shear strength of sands for different sample preparation methods." *Soils Found.* 26 (3): 23–41. https://doi.org/10.3208/sandf1972.26.3_23.
Tokimatsu, K., S. Tamura, H. Suzuki, and K. Katsumata. 2012. "Building damage associated with geotechnical problems in the 2011 Tohoku Pacific earthquake." *Soils Found.* 52 (5): 956–974. https://doi.org/10.1016/j.sandf.2012.11.014.
Travasarou, T., J. M. Chacko, W. Y. Chen, A. Giannakou, M. Ilankatharan, and J. Ugalde. 2012. "Application of advanced numerical methods to assess seismic performance for major projects." In *Proc., 2nd Int. Conf. on Performance-Based Design in Earthquake Geotechnical Engineering*. Santiago, Chile: Chilean Geotechnical Society.
Travasarou, T., W. Y. Chen, and J. M. Chacko. 2011. "Liquefaction induced uplift of buried structures: Insights from the study of an immersed railway tunnel." In *Proc., 5th Int. Conf. on Earthquake Geotechnical Engineering*. Santiago, Chile: Chilean Geotechnical Society.
Umar, M., G. Chiaro, and T. Kiyota. 2016. "On the influence of initial static shear on large deformation behavior of very loose Toyoura sand in undrained cyclic torsional shear tests." In *Proc., 6th Japan-Korea Geotechnical Workshop*. Tokyo: Japanese Geotechnical Society.
Wahyudi, S. 2014. "Cyclic simple shear tests using stacked-ring on multiple liquefaction properties of sands." Ph.D. dissertation, Dept. of Civil Engineering, Univ. of Tokyo.
Wang, R., P. Fu, J. M. Zhang, and Y. F. Dafalias. 2016. "DEM study of fabric features governing undrained post-liquefaction shear deformation of sand." *Acta Geotech.* 11 (6): 1321–1337. https://doi.org/10.1007/s11440-016-0499-8.
Wei, J., and G. Wang. 2017. "Discrete-element method analysis of initial fabric effects on pre- and post-liquefaction behavior of sands." *Géotech. Lett.* 7 (2): 161–166. https://doi.org/10.1680/jgele.16.00147.
Wu, J. 2002. "Liquefaction triggering and post-liquefaction deformation of Monterey 0/30 sand under uni-directional cyclic simple shear loading." Ph.D. dissertation, Dept. of Civil and Environmental Engineering, Univ. of California, Berkeley.
Yang, Z., A. W. Elgamal, and E. Parra. 2003. "Computational model for cyclic mobility and associated shear deformation." *J. Geotech. Geoenviron. Eng.* 129 (12): 1119–1127. https://doi.org/10.1061/(ASCE)1090-0241(2003)129:12(1119).
Yasuda, S., H. Nagase, H. Kiku, and Y. Uchida. 1992. "The mechanism and a simplified procedure for the analysis of permanent ground displacement due to liquefaction." *Soils Found.* 32 (1): 149–160. https://doi.org/10.3208/sandf1972.32.149.
Yen, W. P., G. Chen, I. Buckle, T. Allen, D. Alzamora, J. Ger, and J. G. Arias. 2011. *Post-earthquake reconnaissance report on transportation infrastructure: Impact of the February 7, 2010, offshore Maule earthquake in Chile*. Rep. No. FWWA-HRT-11-030. Washington, DC: Federal Highway Administration.
Yi, F. 2010. "Procedures to evaluate liquefaction-induced lateral spreading based on shear wave velocity." In *Proc., 5th Int. Conf. on Recent Advances in Geotechnical Earthquake Engineering and Soil Dynamics*. Rolla, MO: Missouri Univ. of Science and Technology.
Yoshimine, M., K. Ishihara, and W. Vargas. 1998. "Effects of principal stress direction and intermediate principal stress on undrained shear behavior of sand." *Soils Found.* 38 (3): 179–188. https://doi.org/10.3208/sandf.38.3_179.
Youd, T. L., C. M. Hansen, and S. F. Bartlett. 2002. "Revised multilinear regression equations for prediction of lateral spread displacement." *J. Geotech. Geoenviron. Eng.* 128 (12): 1007–1017. https://doi.org/10.1061/(ASCE)1090-0241(2002)128:12(1007).
Zhang, G., P. K. Robertson, and R. W. I. Brachman. 2004. "Estimating liquefaction-induced lateral displacements using the standard penetration test or cone penetration test." *J. Geotech. Geoenviron. Eng.* 130 (8): 861–871. https://doi.org/10.1061/(ASCE)1090-0241(2004)130:8(861).
Zhang, J. M., Y. Shamoto, and K. Tokimatsu. 1997. "Moving critical and phase-transformation stress state lines of saturated sand during undrained cyclic shear." *Soils Found.* 37 (2): 51–59. https://doi.org/10.3208/sandf.37.2_51.
Zhang, J. M., and G. Wang. 2012. "Large post-liquefaction deformation of sand, part I: Physical mechanism, constitutive description and numerical algorithm." *Acta Geotech.* 7 (2): 69–113. https://doi.org/10.1007/s11440-011-0150-7.
Ziotopoulou, K. 2016. *Cyclic undrained uniform stress-controlled direct simple shear tests on Nevada Sand*. Technical Rep. Davis, CA: Univ. of California, Davis.
Ziotopoulou, K., and R. W. Boulanger. 2016. "Plasticity modeling of liquefaction effects under sloping ground and irregular cyclic loading conditions." *Soil Dyn. Earthquake Eng.* 84 (May): 269–283. https://doi.org/10.1016/j.soildyn.2016.02.013.
Ziotopoulou, K., J. Montgomery, A. M. Parra Bastidas, and B. Morales. 2018. "Cyclic response of Ottawa F-65 sand: Laboratory and numerical investigation." In *Proc., Geotechnical Earthquake Engineering and Soil Dynamics V 2018 (GEESD V)*. Reston, VA: ASCE.
Ziotopoulou, K., J. Montgomery, D. Tsiaousi, P. Tasiopoulou, J. Ugalde, and T. Travasarou. 2019. "Effect of numerical modeling protocols on the seismic response of a liquefiable slope." In *Proc., 7th Int. Conf. on Earthquake Geotechnical Engineering (ICEGE)*. Boca Raton, FL: CRC Press.